Analytical and numerical DDA analysis on the collapse mode of circular masonry arches

Egidio Rizzi [a,*], Fabio Rusconi [a], Giuseppe Cocchetti [a,b]

[a] Università degli Studi di Bergamo, Dipartimento di Ingegneria (Dalmine), viale G. Marconi 5, I-24044 Dalmine (BG), Italy
[b] Politecnico di Milano, Dipartimento di Ingegneria Civile e Ambientale, piazza Leonardo da Vinci 32, I-20133 Milano, Italy

Article history:
Received 25 December 2012
Revised 16 December 2013
Accepted 18 December 2013
Available online 25 January 2014

1. Introduction

This paper presents an analytical and numerical analysis on the collapse mode of circular masonry arches. Specific reference is made here to the so-called *Couplet–Heyman problem* of finding the minimum thickness necessary for equilibrium of a circular masonry arch subjected only to self-weight, Heyman [30,31,32,33]. Extensive historical perspectives on the subject, and related topics, are provided by Heyman himself in his writings and e.g. in Sinopoli et al. [52], Foce [22,23] and, recently, Cecchi [10,11], while a comprehensive discussion on settled and open issues together with additional references to the pertinent literature is provided in Cocchetti et al. [13], which represents a sort of reference, companion paper of the present.

Indeed, this investigation is part of a research program that has been started at the University of Bergamo since 2006 on the analysis of the collapse modes of circular masonry arches (Colasante [14]). First, the derivation of analytical solutions has been attempted, in the spirit of Limit Analysis as applied to masonry structures (see e.g. Kooharian [37]) and along the line traced by Heyman's work, and within his classical behavioural assumptions for the masonry arch, leading to often-quoted classical Heyman's solution. This solution provides the critical characteristic parameters of the symmetric purely-rotational five-hinge collapse mechanism (see Fig. 1), i.e. the unknown angular position β of the intrados hinges at the haunches (e.g. taken from the vertical axis of symmetry at the crown), the minimum thickness (t) to radius (r) ratio $\eta = t/r$ required for equilibrium and the non-dimensional horizontal thrust $h = H/(wr)$ acting in such a limit state, where $w = \gamma td$ is the self-weight per unit centreline of the arch (γ specific weight per unit volume; d out-of-plane depth of the arch). Along this research path, an additional solution has been developed, as independently re-derived here, which is labelled CCR (Cocchetti et al. [13]), together with a Milankovitch-type solution (see Milankovitch [44], as reported by Foce [23]), that accounts for the true location of the centres of gravity of the arch chunks. These solutions are fully consistent with recent results by Ochsendorf [45,46] and Block et al. [6], and a re-discussion by Heyman [33]. Second, numerical simulations by the Discrete Element Method (DEM), within a Discontinuous Deformation Analysis (DDA) computational environment have been performed, to further support the validity of the obtained analytical solutions, with good overall matching of the obtained results (Rusconi [50]). The main (and additional) results coming from this latter investigation are systematically reported here, while a preliminary account was provided in Rizzi et al. [48].

Actually, the whole started by inspecting the work of Bičanič et al. [4], where a numerical analysis of masonry arch bridges based on a DDA method was presented (see also Thavalingam et al. [59]), by making explicit reference to Heyman's results. Since, in their Fig. 7 Bičanič et al. [4] were reporting slightly different values of the critical parameters β and η, with respect to those that

* Corresponding author. Tel.: +39 035 205 2325; fax: +39 035 205 2310.
E-mail address: egidio.rizzi@unibg.it (E. Rizzi).

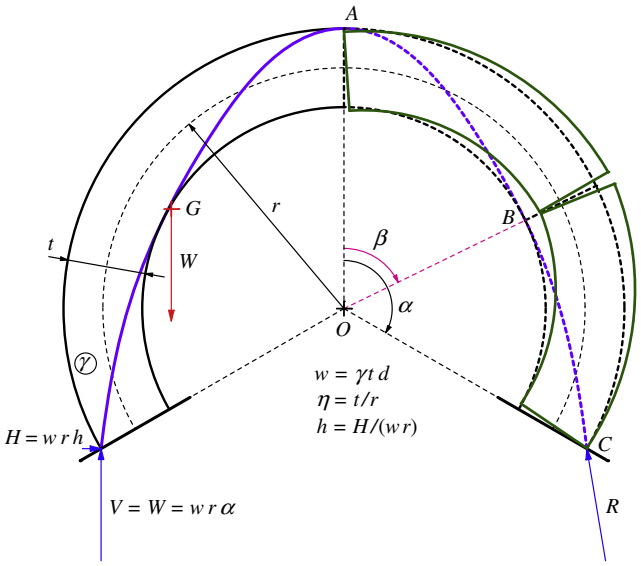

Fig. 1. Analytical sketch of a symmetric circular continuous masonry arch (of specific self-weight γ and out-of-plane depth d), with out-ward rotational collapse mechanism of the half-arch; depicted from the outcomes of CCR solution for the over-complete case of $\alpha = 120°$, in the critical condition of least thickness of the arch: $\beta_{CCR} = 1.11714$ rad $= 64.0072°$, $\eta_{CCR} = 0.326547$, $h_{CCR} = 0.349556$, while $\beta_M = 1.11248$ rad $= 63.7402°$, $\eta_M = 0.327607$, $h_M = 0.342263$ (Milankovitch solution), $\beta_H = 1.31409$ rad $= 75.2920°$, $\eta_H = 0.314124$, $h_H = 0.344942$ (Heyman's solution).

could be directly obtained from Heyman's formulas (recalled later in Section 2), a re-derivation of Heyman's solution was attempted first, which actually led to other slightly-different results. This has driven to enquire in details all the analytical developments, by formalising systematically three analytical solutions (Heyman, CCR, Milankowitch), as now documented extensively in Cocchetti et al. [13]. Then, the attempt of independent validations, e.g. through an appropriate numerical method useful to represent the inherent discrete block structure of the masonry arch, came-up naturally to assess the obtained analytical solutions.

The present numerical analysis makes use of numerical methods that are referred-to as belonging to the family of the Discrete Element Method (DEM), see e.g. Cundall and Hart [18] and, with specific reference to masonry structures, Lemos [39], which provided an excellent overview on several DEM approaches in the structural analysis of masonry. Among the first researchers that appear to have been developing these numerical tools, specifically conceived for solids and structures that are endowed with intrinsic discontinuities, the references of Burman [8], Cundall [16], Maini et al. [43], Cundall and Strack [17] could be cited. Later, Lemos et al. [38], Williams et al. [61], Williams and Mustoe [62], Hahn [29], Shi and Goodman [53,54], Shi [55,56] have further developed the method, according to different formulations. Specifically, Cundall and Hart [18] have provided a revision of the various techniques within this context, where fundamental characteristics have been classified for the Discrete Element Method, such as the ability to allow for finite displacements and rotations of the discrete blocks, including the complete detachment of blocks and the automatic account of activation of new contacts among them. Based on all these premises, four fundamental classes of DEM methods were defined: Distinct Element Method, developed by Cundall [16] himself and co-workers; Modal Methods, developed by Williams et al. [61] and Williams and Mustoe [62]; Discontinuous Deformation Analysis (DDA), proposed by Gen-Hua Shi [55] and further developed as briefly described below; Momentum Exchange Method, outlined by Hahn [29].

The third approach cited above, i.e. the DDA method, is the one that is going to be employed here, since it has been already proved to be specifically efficient in the modelling of the statics of masonry arches, as cited below. It is based on a kinematic description of the block deformation through appropriate kinematic degrees of freedom (displacements and deformations of the block). Different developments on the DDA method have been attempted in the literature, see e.g. Shi and Goodman [53,54], Shi [55,56], Lin et al. [40], Wang et al. [60], Doolin and Sitar [19,20], Yeung et al. [63,64], Jiang and Yeung [35], Jiang et al. [36], which have led by now to many different validation cases (see e.g. MacLaughlin and Doolin [42], with specific citation to the Couplet–Heyman problem) and practical applications in various engineering contexts, including, which is relevant to the present, in the statics of masonry arches (see e.g. Ma et al. [41], Thavalingam et al. [59], Bičanič et al. [4], Tóth et al. [58], with discussion on DEM and DDA methods). The present work attempts to use, as-is, rather than to develop, the DDA method, according to a numerical tool that has been made available in internet, as shortly described in Section 3. Different numerical techniques that could be used as well in the present context are extensively cited and discussed in Cocchetti et al. [13], including recent contributions (e.g. Giordano et al. [27], Drosopoulos et al. [21], Cavicchi and Gambarotta [9], Chen et al. [12], Audenaert et al. [2], Armesto et al. [3], Oliveira et al. [47], Gago et al. [25], Albuerne et al. [1], Gubana and Di Gianantonio [28], Holzer [34], Sacco [51], Solla [57]).

The paper is organised as follows. Section 2 presents a new derivation of the analytical solutions for the purely-rotational mode of circular masonry arches, with general half-angle of embrace $0° < \alpha < 180°$, including over-complete arches ($\alpha > 90°$). As a main difference to the analytical developments in Cocchetti et al. [13], focus is made here on a direct evaluation of the least thickness condition, as then explored in the subsequent numerical DDA derivations. Section 3 presents the main body of the numerical DDA results, which are taken as specific numerical experiments on sample masonry arch models, with great comparison of the obtained numerical results to the theoretical predictions. Section 4 gathers the salient conclusions of the present study.

2. Analytical treatment of the Couplet–Heyman problem

Based on fundamental observations on the behaviour of masonry structures and specifically of masonry arches, Jacques Heyman has nicely formulated the statics of masonry arches by stating the following three basic behavioural assumptions (often quoted-to as the *classical three Heyman's hypotheses*, see e.g. [31 – p. 70, 32 – p. 30]):

1. *sliding failure does not occur*;
2. *masonry has an infinite compressive strength*;
3. *masonry has no tensile strength*.

According to these hypotheses, the arising collapse mode of the symmetric arch is a symmetric purely-rotational mechanism with five hinges (a roller and two hinges for the half-arch), which can be analysed (Fig. 1): one hinge develops at the extrados at crown *A*, two hinges arise at shoulders *C* and two inner hinges appear at, to be determined, haunches *B*. The problem has been studied by different researchers, starting from the so-called pre-elastic theories of the 1700 (see e.g. Heyman [31,32], Sinopoli et al. [52], Foce [22]), with salient developments of specific reference on what is going to be debated here by Milankovitch [44], as described by Foce [23], by Blasi and Foraboschi [5], Boothby [7], Sinopoli et al. [52], Ochsendorf [45,46] and now by the companion work Cocchetti et al. [13].

Heyman [30 – p. 367–368, 31 – p. 79], based on the reasoning described above, has derived the following compact well-know explicit formulas for obtaining the critical characteristic parameters

β, η, h of a circular masonry arch with angle of embrace 2α in the critical condition of least thickness (Fig. 1):

$$\beta\cot\beta\frac{2\beta\cos\beta+\sin\beta\cos^2\beta+\sin\beta}{2\beta\cos\beta+\sin\beta\cos^2\beta-\sin\beta\cos\beta}=\alpha\cot\frac{\alpha}{2}=A(\alpha) \tag{1}$$

$$\eta=\frac{t}{r}=2\frac{(\beta-\sin\beta)(1-\cos\beta)}{\beta(1+\cos\beta)} \tag{2}$$

$$h=\frac{H}{wr}=h_H=\beta\cot\beta \tag{3}$$

From Eq. (1), a numerical solution for β at given half-angle of embrace α derives the angular position of the inner hinge at the haunches, which can then be substituted into Eqs. (2) and (3), to get right-away the thickness to radius ratio η and the horizontal non-dimensional thrust h in the critical condition, respectively. Notice that the dependence on the half-angle of embrace α is inherited through the group $A=\alpha\cot\alpha/2$ appearing in Eq. (1). In Cocchetti et al. [13] a detailed analytical derivation of the formulas above (which seems to be missing in the quoted Heyman's writings) is provided, together with a clear interpretation of their physical meaning. Specifically, Eq. (3) states (uncorrectly) that, in the critical condition of minimum thickness, the resultant thrust force at the haunches B becomes tangent to the intrados of the arch (see recent discussion Heyman [33], in which the Author "*confesses to an error he made in 1969*"). Since this is actually different than stating correctly that the true line of thrust has to become tangent to the intrados there (Fig. 1), see Ochsendorf [45,46], Heyman [33], Cocchetti et al. [13], additional analytical derivations have been considered in view of deriving the truly correct solution in academic terms (differences in engineering terms appear quite limited, at least for η and h, but a bit more readable for β, especially at increasing opening angle of the arch).

With reference to Fig. 2, this leads to write-down the equation of rotational equilibrium of any upper portion of the half-arch with variable angular opening β, with respect to the centre of pressure P, at eccentricity $e(\beta)$ from centreline, towards the centre O of the arch. According to this, one obtains the balance of moments with respect to point P of the horizontal thrust $H=wrh$, acting at crown A and of the self-weight resultant W_1 of the upper portion of the arch, acting at point G_1, at horizontal distance x_1 from crown A and vertical distance y_1 from centre O:

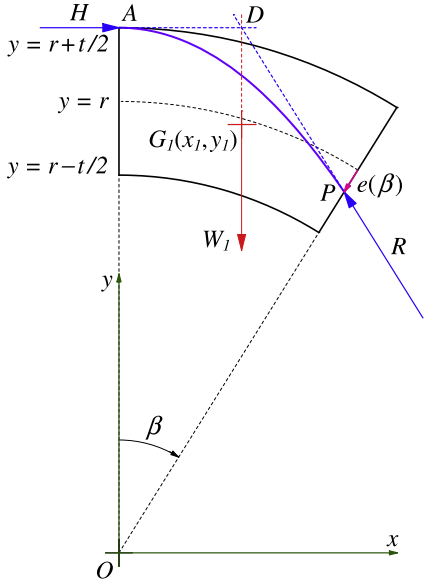

Fig. 2. Analytical representation (CCR solution) of the line of thrust with eccentricity $e(\beta)$ and rotational equilibrium of any upper portion of the half-arch at variable opening β; the lines of action of the three represented forces H, W_1 and R intersect at common point D.

$$H\cdot\left[r+\frac{t}{2}-(r-e)\cos\beta\right]=W_1\cdot[(r-e)\sin\beta-x_1] \tag{4}$$

where

$$W_1=\int_{V_1}\gamma dV=\underbrace{w}_{\gamma td}r\beta,$$
$$x_1=\frac{\int_{V_1}\gamma x\,dV}{\int_{V_1}\gamma dV}=\underbrace{r(1+\delta_M\eta^2/12)}_{r_G}\frac{1-\cos\beta}{\beta}, \tag{5}$$
$$y_1=\frac{\int_{V_1}\gamma y\,dV}{\int_{V_1}\gamma dV}=\overbrace{r(1+\delta_M\eta^2/12)}\frac{\sin\beta}{\beta}$$

and δ_M is just a flag that has been introduced to account for Milankovitch correct self-weight distribution ($\delta_M=1$), rather than for the approximate self-weight distribution according to the standard hypothesis of uniform distribution along the geometrical centreline of the arch ($\delta_M=0$), which characterises both Heyman's and CCR solutions. In other words, Milankovitch solution accounts for the correct location of the centre of gravity of each ideal infinitesimal wedge-shaped voussoir of the arch, at a radial distance $r_G=r(1+\eta^2/12)$ from centre O that is a bit larger than r. The effect of the correction term $\eta^2/12$, with respect to 1, is quadratic in η, thus is expected to be not that relevant, at least until η keeps small. In practice, the differences between Milankovitch ($\delta_M=1$) and CCR ($\delta_M=0$) solutions are awaited to be quite marginal in engineering terms, as indeed confirmed in the sequel.

By inserting the expressions of W_1 and x_1 in Eq. (5) into Eq. (4) and solving with respect to the non-dimensional horizontal thrust $h=H/(wr)$ one has the value of the non-dimensional thrust that warrants rotational equilibrium in the sense above:

$$h=\frac{\left(2-\frac{2e}{t}\eta\right)\beta\sin\beta-2(1-\cos\beta)(1+\delta_M\eta^2/12)}{2+\eta-\left(2-\frac{2e}{t}\eta\right)\cos\beta} \tag{6}$$

Two specific cases from Eq. (6) must be mentioned. The first is the case where β denotes the position of the inner hinge B at the intrados at the haunches, where $e=t/2$, thus with non-dimensional eccentricity $\hat{e}=2e/t=1$, which states the rotational equilibrium of the upper portion AB of the half-arch in Fig. 1, leading to the so-called *lower thrust* Heyman [31,32], Blasi and Foraboschi [5], Cocchetti et al. [13]:

$$h=h_1=\frac{(2-\eta)\beta\sin\beta-2(1-\cos\beta)(1+\delta_M\eta^2/12)}{2+\eta-(2-\eta)\cos\beta}=\frac{num_{h_1}}{den_{h_1}} \tag{7}$$

The second is the case where $\beta=\alpha$ marks the full half-opening of the arch, with hinge C at the extrados at the shoulders of the arch, where $e=-t/2$, thus with non-dimensional eccentricity $\hat{e}=2e/t=-1$, which practically states the rotational equilibrium of the total half-arch AC in Fig. 1:

$$h=h_2=\frac{(2+\eta)\alpha\sin\alpha-2(1-\cos\alpha)(1+\delta_M\eta^2/12)}{(2+\eta)(1-\cos\alpha)}$$
$$=A(\alpha)-\frac{2}{2+\eta}(1+\delta_M\eta^2/12) \tag{8}$$

where as already remarked in Heyman's Eq. (1), the group $A(\alpha)$ resumes the implicit dependence on the half-opening angle α (which is a common characteristic feature of all the analytical solutions derived here):

$$A(\alpha)=\frac{\alpha\sin\alpha}{1-\cos\alpha}=\alpha\cot\frac{\alpha}{2} \tag{9}$$

Otherwise, by solving equilibrium Eq. (4) with respect to the eccentricity e or to the non-dimensional eccentricity $-1\leqslant\hat{e}=2e/t\leqslant 1$ one gets:

$$\hat{e}(\beta) = \frac{2e(\beta)}{t} = \frac{2\beta\sin\beta - 2(1-\cos\beta)(1+\delta_M\eta^2/12) - h(2+\eta-2\cos\beta)}{\eta(\beta\sin\beta + h\cos\beta)} \tag{10}$$

which provides the position of the line of thrust along the arch (as already represented analytically in Figs. 1 and 2). Eqs. (6) and (10) are synonymously stating the rotational equilibrium of any upper portion of the arch with general angular opening β (Fig. 2). Obviously, according to what has been derived above, Eq. (7), that is $h = h_1$, and Eq. (8), namely $h = h_2$, could be obtained from Eq. (10) by setting respectively $\hat{e} = 1$ at β and $\hat{e} = -1$ at $\beta = \alpha$, and then solving with respect to h.

Actually, one may also insert $h = h_2$ in Eq. (10), so that to build-in the property that $\hat{e}(\alpha) = -1$, at any given value of half-opening angle α of the arch, giving rise to:

$$\hat{e}(\beta) = \frac{2e(\beta)}{t} = \frac{2(2+\eta)\Big(\beta\sin\beta-(1-\cos\beta)A\Big) - \eta\Big((2+\eta)A - 2\cos\beta(1+\delta_M\eta^2/12)\Big)}{\eta(2+\eta)\Big(\beta\sin\beta-(1-\cos\beta)A\Big) + \eta\Big((2+\eta)A - 2\cos\beta(1+\delta_M\eta^2/12)\Big)} \tag{11}$$

which represents the position of any line of thrust in respect of equilibrium, passing from both crown A and shoulder C, at any half-opening α (thus at any $A = \alpha\cot\alpha/2$) and thickness to radius ratio η of the circular arch.

This immediately reveals that, at given α, the value of η may lead to (see Fig. 3, where the typical case of the complete semi-circular arch, $\alpha = 90°$, is reported): super-critical conditions, where the line of thrust is comfortably contained within the arch profile; critical condition of least thickness, where the line of thrust becomes truly tangent to the intrados at the haunches (see also Fig. 1); sub-critical conditions, which would lead to unfeasible lines of thrust going-out of the arch profile, thus violating Heyman's hypothesis-3 of no tensile strength of the masonry arch.

So far only equilibrium equations have been considered. In order to address the critical condition of minimum thickness, the tangency condition of the line of thrust to the intrados at the haunches B (where $\hat{e} = 1$) should be formalised in analytical terms. This equivalently leads to state either the stationary condition $e'(\beta) = 0$, on the eccentricity e (or $\hat{e}$), from Eq. (10), or the stationary condition $h_1'(\beta) = 0$, on the lower thrust h_1, from Eq. (7) (Cocchetti et al. [13]). It can be checked that, given the fractional forms in Eqs. (7) and (10), and derivatives that can be derived accordingly, this leads to:

$$\begin{aligned} h = h_e &= \frac{num'_{h_1}}{den'_{h_1}} \\ &= \frac{(2-\eta)(\sin\beta+\beta\cos\beta) - 2\sin\beta(1+\delta_M\eta^2/12)}{(2-\eta)\sin\beta} \\ &= \beta\cot\beta - \frac{\eta-2+2(1+\delta_M\eta^2/12)}{2-\eta}\delta_{CCR} \\ &= \overbrace{\beta\cot\beta}^{h_H} - \frac{\eta}{2-\eta}\delta_{CCR}(1+\delta_M\eta/6) \end{aligned} \tag{12}$$

where δ_{CCR} is another flag that has been introduced in the last expressions in Eq. (12) to allow shifting from CCR and Milankovitch solutions ($\delta_{CCR} = 1$), stating the true tangency condition on the line of thrust, to Heyman's solution ($\delta_{CCR} = 0$), stating the incorrect (say approximate) tangency condition on the resultant thrust force. Note that, despite h_e, Eq. (12), differs from Heyman's h_H, Eq. (3),

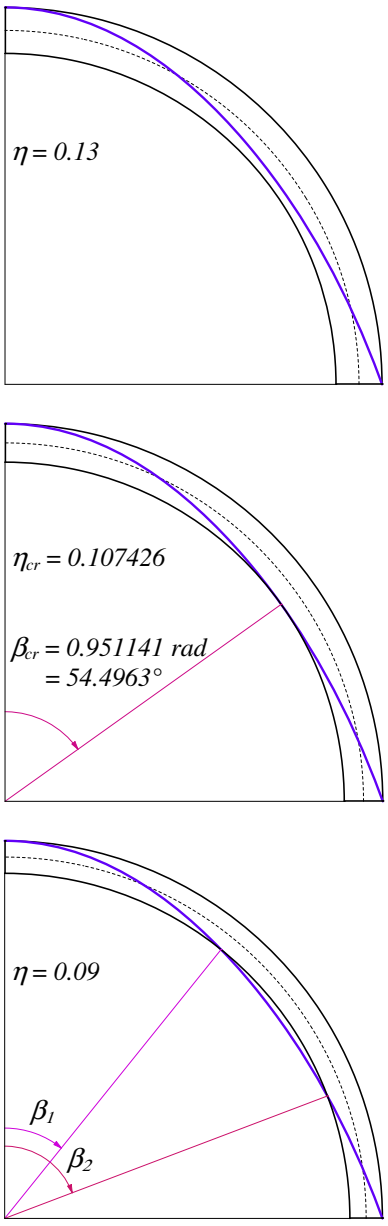

Fig. 3. Analytical plots of the line of thrust of the complete semi-circular arch ($\alpha = 90°$) in super-critical, critical and sub-critical conditions (CCR solution); see also next Fig. 4.

their difference is ruled again by parameter η, thus is expected to be quite minimal, at least until η keeps small.

In sum, the final system of three equations (two equilibrium equations and one tangency condition) leading to the solution of the Couplet–Heyman problem in the characteristic unknowns β, η, h, at given $A(\alpha)$ may thus be cast as follows:

$$\begin{cases} h = h_1 = \dfrac{(2-\eta)\beta\sin\beta - 2(1-\cos\beta)(1+\delta_M\eta^2/12)}{2+\eta-(2-\eta)\cos\beta} \\ h = h_2 = A(\alpha) - \dfrac{2}{2+\eta}(1+\delta_M\eta^2/12) \\ h = h_e = \overbrace{\beta\cot\beta}^{h_H} - \dfrac{\eta}{2-\eta}\delta_{CCR}(1+\delta_M\eta/6) \end{cases} \tag{13}$$

where the couples of flags (δ_{CCR}, δ_M) should be conceived as: (0,0) for Heyman's solution; (1,0) for CCR solution; (1,1) for Milankovitch solution. Notice that the solution that would be obtained for $(\delta_{CCR}, \delta_M) = (0,1)$ would not make much sense, because it would cor-

respond to a Heyman's solution with a true self-weight distribution (though still with an improper tangency condition); thus, this has not been enquired further. It can be readily checked that, by setting $(\delta_{CCR}, \delta_M) = (0,0)$ in system (13), Heyman's formulas (1)–(3) can be re-obtained: Eq. $(13)_c$ becomes the same as Eq. (3); it can be substituted into Eq. $(13)_a$, which can be solved with respect to η, leading to Eq. (2); this obtained one and again Eq. $(13)_c$ are inserted into Eq. $(13)_b$ and solved with respect to A, leading to Eq. (1). Detailed analytical representations of CCR and Milankovitch solutions are instead provided in Cocchetti et al. [13]. Further aspects and new additional interpretations on these solutions are derived here in the next subsection.

2.1. Direct derivation of least thickness

System (13) can be directly solved for the triplet β, η, h. However, further insight into the derivation of the critical condition of least thickness could be gained by an independent treatment of the tangency condition $(13)_c$.

By eliminating the non-dimensional horizontal thrust h (that is expected to be non-negative, $h \geqslant 0$, in view of Heyman's hypothesis-3) from the first two relations in system (13), i.e. by stating a single equilibrium relation from subsystem $\{h = h_1,\ h = h_2\}$ as $h_1 = h_2$, or either by setting $\hat{e} = 1$ at β in Eq. (11), one obtains the following solving (up to cubic) polynomial equilibrium equation in η and β:

$$pol_{\eta}^{equil} = \delta_M C\eta^3 - 3(\beta S + (1+C)A)\eta^2 + 12(C-A)\eta + 12(\beta S - (1-C)A) = 0 \tag{14}$$

where for the sake of compactness, $S = \sin\beta$ and $C = \cos\beta$. Notice that obtained equilibrium Eq. (14) is cubic for Milankovitch solution ($\delta_M = 1$) and quadratic for CCR/Heyman's solutions ($\delta_M = 0$). Also, these equilibrium states in terms of η, which are meaningful as well only for $\eta \geqslant 0$, hold only whereby the concomitant thrust is non-negative, $h \geqslant 0$, i.e. from Eq. $(13)_b$, where $h = h_2 \geqslant 0$. This leads, respectively for CCR/Heyman's ($\delta_M = 0$) and Milankovitch solutions ($\delta_M = 1$), to lower-bound values of η:

$$\eta_0^{CCR/H} = 2\left(\frac{1}{A} - 1\right) \leqslant \eta;$$
$$\eta_0^{M} = 3\left(A - \sqrt{(A+2)(A-2/3)}\right) \leqslant \eta \leqslant 3\left(A + \sqrt{(A+2)(A-2/3)}\right) \tag{15}$$

The solution of Eq. (14) can be handled analytically. An explicit representation for Milankovitch solution ($\delta_M = 1$) coming from the solution of a true cubic equation is too lengthy to be reported here (though it can be handled analytically in plot form, as represented below). In CCR and Heyman's cases ($\delta_M = 0$) things are a bit simpler, since Eq. (14) becomes quadratic. The explicit solution of Eq. (14) can then be reported compactly in this latter case, in its meaningful branch ($\eta \geqslant 0$):

$$\eta^{CCR/H} = 2\frac{C - A + \sqrt{C(C-(2-CA)A) + \beta S(\beta S + 2CA)}}{\beta S + (1+C)A} \tag{16}$$

In both cases the meaningful solution branch $\eta(\beta)$ of Eq. (14), satisfying $\eta \geqslant 0$ and relations (15), i.e. $h \geqslant 0$, traces the function $\eta(\beta)$, at given $A(\alpha)$, that corresponds to equilibrium states of the arch. It actually represents the limit value of thickness to radius ratio η leading to collapse at a given location β of the inner intrados hinge. Notice that, at any given sub-critical $\eta_0 \leqslant \eta < \eta_{cr}$, there are two values of inner hinge location β corresponding to the same η. On the other hand, for $\eta > \eta_{cr}$ no inner hinges form (super-critical condition, i.e. no rotational collapse) and exactly at $\eta = \eta_{cr}$ just a single intrados hinge forms, which really states the critical condition of least thickness as leading to the maximum value of η at variable hinge location β. A representation on this is reported in Fig. 4 for $\eta(\beta)$ from Eq. (16), for the case of the complete semi-circular arch ($\alpha = 90°$). All these considerations have relevant implications in what is going to be reported numerically in Section 3 and fully agree with what has been already illustrated in Fig. 3, in terms of the line of thrust in super-critical, critical and sub-critical conditions.

Different plots of equilibrium function $\eta(\beta)$ from Eq. (16) are represented for CCR solution in Fig. 5, for various cases of half-angle of embrace α, specifically at variable $A = \alpha\cot\alpha/2$ from $A = 2$ ($\alpha = 0$) down to $A_l^{CCR} = 2/3\,(\alpha_l^{CCR} = 2.64839\ \text{rad} = 151.742°)$, which corresponds to the limit of validity of CCR solution, leading to $\eta_l^{CCR} = 1$ and $h_l = 0$ in the critical condition Cocchetti et al. [13]. The characteristic case of $A = 1$ ($\alpha = 2.33112\ \text{rad} = 133.563°$), which separates the behaviour of $\eta(\beta)$ near $\beta \to 0$, as discussed below, is also reported, as well as the case of $A = A_{s\beta}^{CCR} = 1.09292\,(\alpha_{s\beta}^{CCR} = 2.23031\ \text{rad} = 127.788°)$, leading to the maximum value of hinge position β, $\beta_{s\beta}^{CCR} = 1.12909\ \text{rad} = 64.6918°$, at variable α. The envelope of the stationary points of equilibrium curve $\eta(\beta)$ represents the final solution curve $\eta(\beta)$ corresponding to critical conditions, as analytically represented in Cocchetti et al. [13].

Furthermore, plots of $\eta(\beta)$ from the solution of Eq. (14) (or again directly from Eq. (16) for CCR/Heyman's solutions) are reported in Figs. 6 and 7 for the two cases of half-angle of embrace $\alpha = 90°$ and $\alpha = 140°$. Notice that, despite that the curve $\eta(\beta)$ representing the

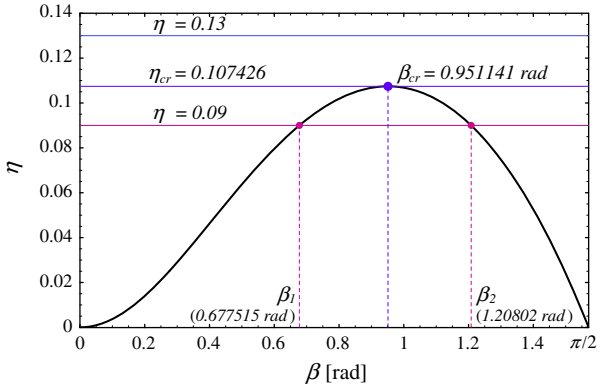

Fig. 4. Analytical plot of the curve $\eta(\beta)$ necessary for equilibrium at given angular position β of the intrados hinge for the complete semi-circular arch ($\alpha = 90°$), with reference to super-critical, critical and sub-critical conditions in Fig. 3 (CCR solution).

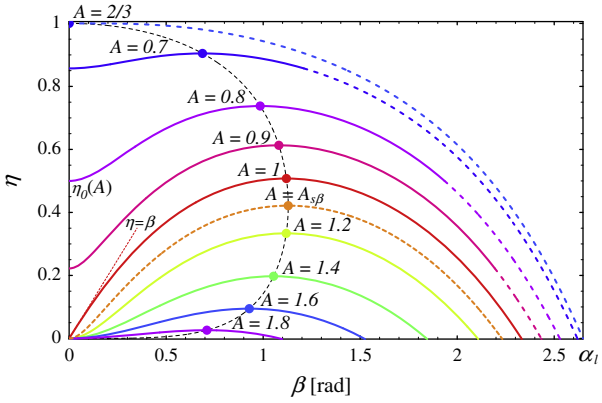

Fig. 5. Analytical plot of the curves $\eta(\beta)$ necessary for equilibrium at given angular position β of the inner hinge, for various arch openings $A = \alpha\cot\alpha/2$ (CCR solution).

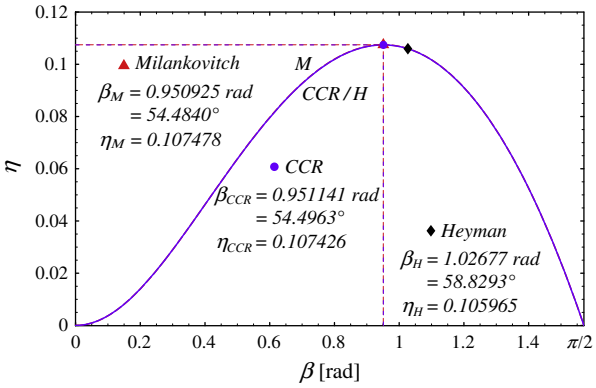

Fig. 6. Analytical plots of $\eta(\beta)$ necessary for equilibrium at given intrados hinge β ($\alpha = 90°$); critical condition of least thickness reached at the stationary point.

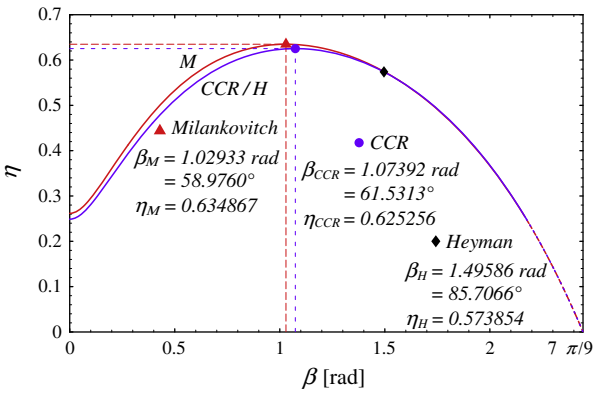

Fig. 7. Analytical plots of $\eta(\beta)$ necessary for equilibrium at given intrados hinge β ($\alpha = 140°$); critical condition of least thickness reached at the stationary point.

equilibrium states for $\delta_M = 0$ is the same for Heyman's and CCR solutions, Heyman's solution does not collocate itself on the true (rather flat) peak of the curve $\eta(\beta)$. Actually, the flatness of the peak explains the rather insensitive effect of the inner hinge position β in stating the correct least thickness η in the critical condition (Heyman [31,32]; for this reason, despite missing the correct location of the inner hinge, Heyman's solution still provides an accurate (though sub-critical) estimate of the thickness to radius ratio η. Moreover, the small difference between the curve $\eta(\beta)$ for CCR/Heyman's solutions and the curve $\eta(\beta)$ for Milankovitch solution can be hardly appreciated in Fig. 6 ($\alpha = 90°$), just a bit more in Fig. 7 ($\alpha = 140°$), which shows that the traditional hypothesis of assuming the self-weight distribution along the geometrical centreline of the arch looks fairly reasonable in practical terms. Also, it is worthwhile to mention again that it is not this specific aspect of selected weight distribution that explains the difference between Heyman's and CCR solutions, which rather sits in the different tangency conditions assumed from scratch at the haunches' intrados Ochsendorf [45,46], Heyman [33], Cocchetti et al. [13].

As stated (just in words) by Heyman, the critical condition of least thickness can now be fully formalised analytically. It is reached by the stationary point (local maximum) of the equilibrium curve $\eta(\beta)$ that is implicitly represented by Eq. (14), since "*the value of β must be chosen to maximise the value of t /r, and this leads eventually to the correct solution*" [30 – p. 368]). In general terms of both Milankovitch and CCR solutions, attached to Eq. (14), this can be handled as follows. Differentiation of Eq. (14) with respect to β yields:

$$\begin{aligned}\frac{dpol_\eta^{equil}}{d\beta} &= \frac{\partial pol_\eta^{equil}}{\partial\beta} + \frac{\partial pol_\eta^{equil}}{\partial\eta}\frac{d\eta}{d\beta}\\ &= \delta_M C'\eta^3 - 3\Big(\beta S + (1+C)A\Big)'\eta^2 + 12\Big(C-A\Big)'\eta\\ &\quad + 12\Big(\beta S - (1-C)A\Big)' + \Big(3\delta_M C\eta^2 - 6\Big(\beta S + (1+C)A\Big)\eta\\ &\quad + 12(C-A)\Big)\eta' = 0\end{aligned} \tag{17}$$

Since by seeking the stationary point one has to set $\eta' = 0$, the term $\partial pol_\eta^{equil}/\partial\beta$ in the second line of Eq. (17) has to vanish at the stationary condition, leading to a further (up to cubic) polynomial stationary condition in η and β:

$$pol_\eta^{stat} = \frac{\partial pol_\eta^{equil}}{\partial\beta} = -\delta_M S\eta^3 - 3(S+\beta C - SA)\eta^2 - 12S\eta + 12(S+\beta C - SA) = 0 \tag{18}$$

which could be taken as stationary condition on the equilibrium path $\eta(\beta)$, where $pol_\eta^{equil} = 0$.

This holds true where the pre-multiplying factor of η' in the last line of Eq. (17), namely $\partial pol_\eta^{equil}/\partial\eta$, keeps non-zero, leading to:

$$\begin{aligned}\eta' = \frac{d\eta}{d\beta} &= -\frac{\frac{\partial pol_\eta^{equil}}{\partial\beta}}{\frac{\partial pol_\eta^{equil}}{\partial\eta}} = -\frac{pol_\eta^{stat}}{\frac{\partial pol_\eta^{equil}}{\partial\eta}}\\ &= -\frac{-\delta_M S\eta^3 - 3\Big(S+\beta C - SA\Big)\eta^2 - 12S\eta + 12\Big(S+\beta C - SA\Big)}{3\delta_M C\eta^2 - 6\Big(\beta S + (1+C)A\Big)\eta + 12\Big(C-A\Big)}\end{aligned} \tag{19}$$

i.e., by setting to zero the denominator in Eq. (19) and solving linearly with respect to A, for non-singular cases that are marked by:

$$A \neq A_{sing} = \frac{\delta_M C\eta^2 - 2\beta S\eta + 4C}{4 + 2(1+C)\eta} \tag{20}$$

It can be checked that $pol_\eta^{equil} = 0$ at $A = A_{sing}$ is satisfied just in the limit $\beta \to 0$, whereby:

$$\begin{aligned}&A_{sing} \to \frac{4+\delta_M\eta^2}{4(1+\eta)},\\ &pol_\eta^{equil} \to \big(\delta_M\eta^2 - 6A\eta + 12(1-A)\big)_{A=A_{sing}}\eta = -\frac{\delta_M\eta^2 + 4\delta_M\eta - 12}{2(1+\eta)}\eta^2\end{aligned} \tag{21}$$

leading to $\eta_{sing} = 0$, $A_{sing} = 1$ as the only singular case of the stationary condition in the solution domain $0 \leqslant \eta \leqslant \eta_l$ ($\eta_l^{CCR} = 1$; $\eta_l^M = 2(2\sqrt{3} - 3) = 0.928203$), $2 \geqslant A \geqslant A_l\Big(A_l^{CCR} = 2/3; A_l^M = \sqrt{3} - 1 = 0.732051\Big)$. Since $pol_\eta^{stat} = 0$ in Eq. (18) is always satisfied for $\beta \to 0$, this means that the curve $\eta(\beta)$ is always flat at $\beta \to 0$, except exactly for $A = 1$. In that case, the expression of η' in Eq. (19) becomes undetermined as 0/0 for $\beta \to 0$, $\eta \to 0$, since also the term $(C - A)$ tends to 0 as $\beta \to 0$ and $A = 1$. By further working-out η' in Eq. (19) through L'Hospital's rule, it can be checked that, in the limit $\beta \to 0$, $\eta \to 0$, at $A = 1$, $\eta' \to 2/A - 1 = 1$, so that the equilibrium curve $\eta(\beta)$ for $A = 1$ is inclined as $\eta = \beta$ at the origin $\eta = 0$, $\beta = 0$ (Fig. 5). This issue is also further commented below.

Now, by further eliminating η from the system $\Big\{pol_\eta^{equil} = 0,\ pol_\eta^{stat} = 0\Big\}$ of two Eqs. (14) and (18), one may reduce it to:

$$\begin{aligned}&S^2\Big(3(\beta + SC) - \frac{3+\delta_M}{2}S\Big)A^3\\ &+ 3\Big((1-C)(\beta - S) - \frac{1-\delta_M}{2}S\Big)(\beta + SC)SA^2\\ &- 3\Big(S + \beta C - \frac{1-\delta_M}{2}S\Big)(\beta + SC)^2A + \frac{3+\delta_M}{2}(\beta + SC)^3 = 0\end{aligned} \tag{22}$$

This provides the solving equation for the angular inner hinge position β at given $A(\alpha)$ in the critical condition (or conversely the half-opening value α, from unknown $A(\alpha)$, at given hinge location β), directly for Milankovitch solution ($\delta_M = 1$, cubic equation):

$$S^2\Big(3(\beta+SC)-2S\Big)A^3+3(1-C)(\beta-S)(\beta+SC)SA^2 - 3(S+\beta C)(\beta+SC)^2A+2(\beta+SC)^3=0 \tag{23}$$

and indirectly for CCR solution, since Eq. (22) can be further reduced to ($\delta_M = 0$, quadratic equation):

$$S\Big(2(\beta+SC)-S\Big)A^2-2(S+\beta C)(\beta+SC)A+(\beta+SC)^2=0 \tag{24}$$

Obtained Eqs. (23) and (24) are fully consistent with what could be derived directly by eliminating the couple η, h from system (13) for Milankovitch and CCR solutions (see Cocchetti et al. [13]).

Once the inner hinge position β is known at given $A(\alpha)$, to get the critical value of η one may solve Eq. (14) at that $A(\alpha)$, at the corresponding critical value of β, as obtained from Eqs. (23) and (24) above. Alternatively, by further eliminating A from the system $\left\{pol_\eta^{equil}=0, pol_\eta^{stat}=0\right\}$ of two Eqs. (14) and (18), one obtains the polynomial equation:

$$\delta_M S\eta^3+3(1+C)(\beta+S)\eta^2-12(\beta+SC-S)\eta+12(1-C)(\beta-S)=0 \tag{25}$$

which allows to represent directly both Milankovitch ($\delta_M = 1$, cubic equation) and CCR ($\delta_M = 0$, quadratic equation) solutions in terms of η, at the critically-obtained β.

Notice that, as illustrated in Figs. 4–7 for the equilibrium curves $\eta(\beta)$, when approaching $\beta \to 0$, from Eq. $(13)_a$ at $\beta \to 0$ one has $h = h_1 = 0$, thus setting $h = h_2 = 0$ in Eq. $(13)_b$ leads to the value η_0 of $\eta(\beta)$ at $\beta \to 0$ which, in conjunction with what derived earlier in Eq. (15), can be stated as:

$$\begin{aligned} &for \quad 1 \leqslant A \leqslant 2: \quad \eta_0 = 0 \\ &for \quad A_l \leqslant A \leqslant 1: \quad \eta_0^{CCR/H} = 2\left(\tfrac{1}{A}-1\right); \\ &\qquad\qquad\qquad\quad \eta_0^{M} = 3\left(A-\sqrt{(A+2)(A-2/3)}\right) \end{aligned} \tag{26}$$

which is zero for $A \geqslant 1$, i.e. for $\alpha \leqslant 2.33112$ rad = 133.563° (including standard cases of complete and under-complete arches with $\alpha \leqslant 90°$ and also cases of over-complete arches with $\alpha > 90°$) and positive for $A < 1$ (corresponding to more unusual cases of over-complete arches with $\alpha > 133.563°$). The value of η_0 for CCR solution in Eq. (26) is also consistent with Eq. (16), in the limit of $\beta \to 0$, since this leads to $\eta_0 = 1/A - 1 + |1/A - 1|$, with same results. Equivalently, from Eq. (14), $pol_\eta^{equil} = 0$, at $\beta \to 0$ one gets:

$$pol_\eta^{equil} \to \left(\delta_M\eta_0^2-6A\eta_0+12(1-A)\right)\eta_0=0 \tag{27}$$

thus $\eta_0 = 0$ is always a solution (meaningful for $A \geqslant 1$) and the other solutions $\eta_0 \geqslant 0$ in Eq. (26) (meaningful for $A \leqslant 1$) are obtained by setting to zero the (up to quadratic) polynomial term within parentheses in Eq. (27).

Also, from the stationary condition as discussed earlier, see Eq. (19), one sees that, for $\beta \to 0$, $\eta'(0) = 0$, if $A \neq 1$, thus the curve $\eta(\beta)$ is always flat at $\beta \to 0$, except for $A = 1$, where the local slope at $\eta_0 = 0$ turns-out equal to 1 (Fig. 5). This can be confirmed also by calculating directly the derivative of the explicit representation of $\eta(\beta)$ in Eq. (16) for CCR/Heyman's solutions or of the meaningful solution $\eta(\beta)$ coming from the implicit cubic representation in Eq. (14) for Milankovitch case. Recall that the condition $\eta = \eta_0$ is a limit state of equilibrium for $A \leqslant 1$, since it leads to a vanishing horizontal thrust ($h = 0$): for $\eta < \eta_0$ equilibrium is no longer possible, since this would lead to negative values of the thrust (thus the curves $\eta(\beta)$ for $A \leqslant 1$ are then indicated by dotted lines in Figs. 5 and 7 as $\eta < \eta_0$).

Also, on the other theoretical extreme $\beta \to \alpha$ of the curve $\eta(\beta)$, it results that $\eta = 0$ (Fig. 5). Indeed from $pol_\eta^{equil} = 0$, Eq. (14), the last polynomial term vanishes and thus $\eta = 0$ is always a solution (though meaningful only for $A \geqslant 1$, since for $A \leqslant 1$ the requirement $\eta \geqslant \eta_0$ arises, to warrant $h \geqslant 0$). This is also confirmed by the fact that the condition $h_1 = h_2$ at $\eta = 0$, solved with respect to A, gives $A = \beta S/(1 - C) = B$, which is indeed satisfied at $\beta = \alpha$.

System (13) or Eqs. (22)–(25) can be used to calculate the critical values of β and η for CCR and Milankovitch solutions, for different values of the half-angle of embrace α, that will be reported in the next section for quantitative comparisons to the numerical results achieved by independent numerical experiments carried-out by the DDA method.

3. Numerical simulations by a DDA formulation

This section reports the core numerical results of the present paper, obtained by a DDA formulation that was freely downloaded from the internet (*sourceforge.net, DDA for Windows, Limerick Version 1.6*). This computer program has been developed by different researchers at the University of Berkeley, among them Doolin and Sitar [19,20], MacLaughlin and Doolin [42]. Despite the limited capabilities of the available tool, quite a few results have been derived, with reference to the guideline trends experienced by the previously-described analytical solutions.

Fundamental aspects that should lay behind the available DDA formulation could be traced-back to the work of Shi and co-workers, see e.g. Shi [55,56] and to the documented contributions of Doolin and Sitar [19,20]. The DDA method introduces appropriate kinematic variables $\boldsymbol{D} = \{u_0, v_0, r_0, \varepsilon_x, \varepsilon_y, \gamma_{xy}\}^T$ as degrees of freedom of the discrete block (displacements, rotation and constant block deformations) and attempts the solution of standard equations of motion in the usual form $\boldsymbol{M}\cdot\ddot{\boldsymbol{D}} + \boldsymbol{C}\cdot\dot{\boldsymbol{D}} + \boldsymbol{K}(\boldsymbol{D})\cdot\boldsymbol{D} = \boldsymbol{F}(t, \boldsymbol{D})$, where $\boldsymbol{M}$, $\boldsymbol{C}$ and $\boldsymbol{K}$ are the assembled mass, damping and stiffness matrices of the discrete system of blocks and $\boldsymbol{F}$ is the vector of external actions. Time integration is basically carried-out in an implicit context by instances of the Newmark method (e.g. Wang et al. [60], Doolin and Sitar [20]), where the time step is set automatically within the step-by-step integration procedure, while the contact among blocks is handled by appropriate algorithms based on penalty methods Lin et al. [40], Doolin and Sitar [19], which also control automatically the penalty constant ruling contact stiffness and block interpenetration.

The numerical results that are reported below have considered different numerical experiments on discretised circular masonry arches with no tensile strength and with no cohesion at the joints (i.e. no mortar). Despite that the investigated Couplet–Heyman problem is ruled just by geometrical characteristics, standard mechanical properties of masonry materials have been imposed into the numerical simulations, namely: Young's modulus 5×10^6 kN/m^2; Poisson's ratio 0.2; specific weight $\gamma = 22$ kN/m^3; mass density 2.24×10^3 kg/m^3. Simulations have been run as "quasi-static", plane stress analyses, with mean radius $r = 10$ m and thickness $t = \eta r$ represented in terms of the thickness to radius ratio η; out-of-plane depth is taken unitary by the program, $d = 1$ m.

Concerning the present "quasi-static" simulations, according to the documentation manual of the adopted DDA program, the following information should be recorded (Doolin and Sitar [20]): *The formulation is transient and fully dynamic. Large displacements and deformations are the result of accumulation of displacements and deformations over a number of small timesteps. However, there is an option to conduct a pseudo-static analysis, in which the block velocities are reset to zero at the start of each timestep.* Thus,

simulations shall be run as normal dynamic ones, through Newmark (average acceleration) time integration, but by setting to zero the initial velocity at the beginning of each time step. Such approximation looks quite appropriate for describing the present target analysis on the statics of circular masonry arches, with specific reference to the characterisation of the onset of the least thickness condition.

Concerning the handling of contact among the blocks through penalty methods the following documentation should be reported (Shi [55,56], Lin et al. [40], Doolin and Sitar [19]): *The kinematical constraints of the block system are imposed using the penalty method. Contact detection is performed in order to determine which block vertices are in contact with edges and vertices of other blocks. Numerical penalties analogous to stiff springs are applied at the contacts to prevent interpenetration of the blocks. Tension or penetration at the contacts will result in expansion or contraction of these "springs," which adds energy to the block system. Thus, the minimum energy solution is one with no tension or penetration.* Though the stiffness of such stiff penalty springs shall play a role in the accuracy of dynamical analyses, such parameter is ruled automatically by the program, together with the handling of the time step, and in the end shall have minor implications in the outcomes of the present framework of characterising the onset of static collapse of the arch. Further documentation on the background of the adopted DDA formulation and details on the implementation of the various arch models are reported in the Laurea Thesis of Rusconi [50 – Chapters 3–4, p. 28–118]. Additional issues and remarks are outlined below.

The present numerical simulations are "quasi-static" as said above and the self-weight is applied as a given load acting on the structure at the initial stage, like in a theoretical de-centering approach. In the spirit of the Couplet–Heyman problem, as codified by Heyman, the point is to see if the arch, with its implemented thickness is able to withstand its self-weight or if it collapses, in the sense that a clear transition to a dynamic response leading to failure of the arch arises, as it can be seen visually in the

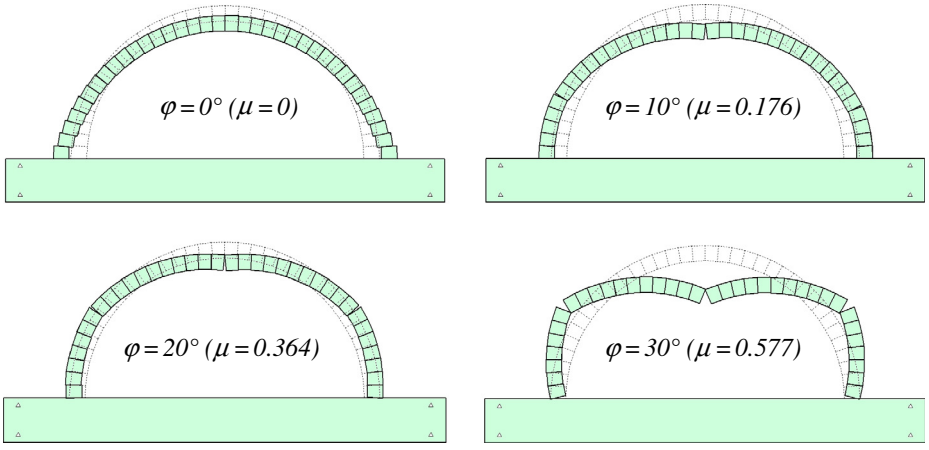

Fig. 8. DDA collapse modes of a complete semi-circular masonry arch ($\alpha = 90°$) with implemented thickness to radius ratio $\eta = \eta_H = 0.105965$, made with 36 blocks (voussoirs with 5° opening), at variable angle of friction φ at the joints (coefficient of friction $\mu = \tan\varphi$).

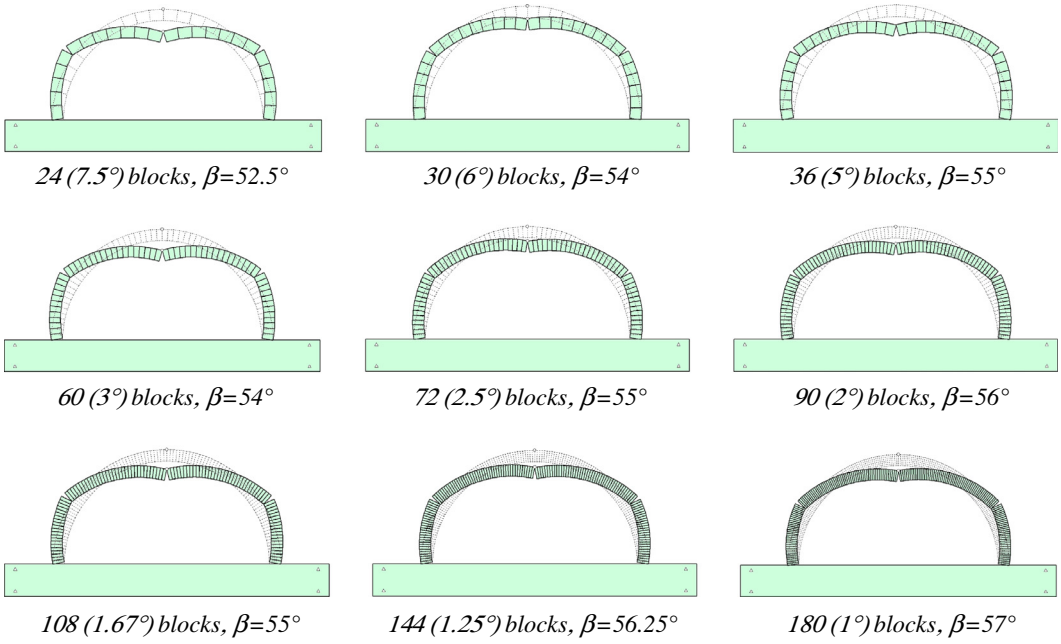

Fig. 9. DDA collapse modes of a complete semi-circular masonry arch ($\alpha = 90°$) with implemented $\eta = \eta_H = 0.105965$ or $\eta = \eta_{CCR} = 0.107426$, made with variable number of blocks (voussoirs with different opening) and recorded angular position β of the inner intrados hinge at the haunches.

simulations. Thus, either the arch stays "stable", basically in the reference configuration, or becomes "unstable" by showing then a collapse response with blocks clearly falling down, through a transition from statics to dynamics.

In the simulations that attempt the least thickness estimation, the arch collapse is detected visually, by changing from the condition of super-critical thickness (where the arch basically stands near to the undeformed configuration) to the condition of sub-critical thickness (where the arch clearly develops a collapse mode leading to the opening of the joints). In seeking such fork of values of critical arch thickness at variable arch thickness, such discontinuous behaviour is clearly detectable visually in running the code. Each simulation starts with a given arch thickness and a statically imposed self-weight. The thickness is varied in each separate simulation, as assigned from scratch, in each single simulation. At the beginning, a quite large thickness is checked, in order to be sure to enforce "stability", by a value much larger than that which could be expected by the theoretical solutions. Then, such thickness is decreased to a value reasonably lower that the critical one, in order to surely experience collapse, as detected above. Then, an intermediate thickness value between these extreme values of arch thickness is attempted, like in a dichotomic method, by producing a series of fork values gradually narrowing down on the true critical thickness of the numerical arch. Each simulation runs separately, with the given thickness and acting self-weight.

It is clear that the present numerical simulations refer to the response of a "true" discrete structure made with blocks. Since Heyman's solution of a continuous arch in the spirit of Limit Analysis shall be ruled just by statics, the simulations attempt to address that, in the sense clarified above. In earlier simulations developed at the time of the Laurea Thesis of Rusconi [50], different Young's moduli (and other material parameters) were tried, from low to very high (also in attempting to address the slight difference in critical thickness prediction that has been subsequently recorded), without revealing any appreciable effects on the estimates of the

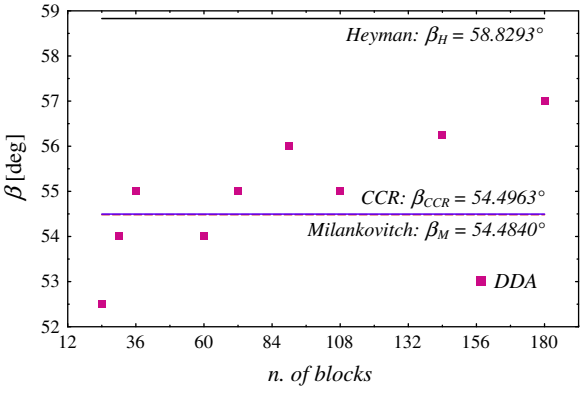

Fig. 10. Same as Fig. 9. DDA recorded angular position β of the inner hinge, with comparison to analytical Heyman, CCR and Milankovitch solutions.

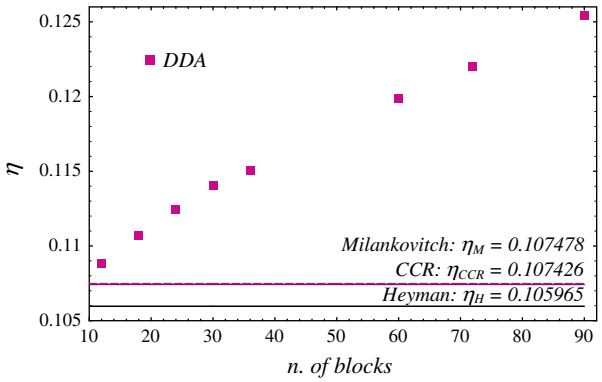

Fig. 11. DDA recorded critical thickness to radius ratio η of a complete semi-circular arch ($\alpha = 90°$) with variable number of blocks (voussoirs with different opening), with comparison to analytical Heyman, CCR and Milankovitch solutions. Results also listed in Table 1.

Table 2
DDA vs. analytical solutions for a complete semi-circular arch ($\alpha = 90°$) made with 4 blocks (see samples in Figs. 12 and 13). Critical thickness to radius ratio η at first collapse instance at so-imposed β joint; results also plotted in Fig. 14.

Hinge position		DDA	Milankovitch		CCR/Heyman	
β		η	$\eta(\beta)$	Δ	$\eta(\beta)$	Δ
(deg)	(rad)	(1)	(1)	(%)	(1)	(%)
10	0.174533	0.0166	0.0108382	53.16	0.0108380	53.16
15	0.261799	0.0293	0.0228544	28.20	0.0228529	28.21
20	0.349066	0.0462	0.0373283	23.77	0.0373224	23.79
25	0.436332	0.0658	0.0527214	24.81	0.0527066	24.84
30	0.523599	0.0835	0.0677042	23.33	0.0676767	23.38
35	0.610865	0.0923	0.0812203	13.64	0.0811788	13.70
40	0.698132	0.1010	0.0924695	9.23	0.0924166	9.29
45	0.785398	0.1077	0.100861	6.78	0.100803	6.84
47.5	0.829031	0.1101	0.103846	6.02	0.103787	6.08
50	0.872665	0.1116	0.105964	5.32	0.105906	5.38
52.5	0.916298	0.1124	0.107179	4.87	0.107124	4.93
54.5	0.951204	0.1123	0.107478	4.49	0.107426	4.54
55	0.959931	0.1122	0.107458	4.41	0.107407	4.46
57.5	1.00356	0.1112	0.106773	4.15	0.106728	4.19
58.8	1.02625	0.1103	0.106027	4.03	0.105985	4.07
60	1.04720	0.1092	0.105099	3.90	0.105060	3.94
65	1.13446	0.1023	0.0986899	3.66	0.0986641	3.69
70	1.22173	0.0912	0.0880599	3.57	0.0880457	3.58
75	1.30900	0.0759	0.0730454	3.91	0.0730395	3.92
80	1.39626	0.0561	0.0534813	4.90	0.0534798	4.90

Table 1
DDA vs. analytical solutions for a complete semi-circular arch ($\alpha = 90°$) made with variable number of blocks. Critical thickness to radius ratio η at first collapse instance; results also plotted in Fig. 11.

N. of blocks	Voussoir opening (deg)	DDA	Milankovitch	CCR	Heyman
			$\eta_M = 0.107478$	$\eta_{CCR} = 0.107426$	$\eta_H = 0.105965$
		η_{DDA}	$(\eta_{DDA} - \eta_M)/\eta_M$	$(\eta_{DDA} - \eta_{CCR})/\eta_{CCR}$	$(\eta_{DDA} - \eta_H)/\eta_H$
		(1)	(%)	(%)	(%)
12	15	0.10884	1.27	1.32	2.71
18	10	0.11068	2.98	3.03	4.45
24	7.5	0.11242	4.60	4.65	6.09
30	6	0.11405	6.11	6.17	7.63
36	5	0.11505	7.05	7.10	8.57
60	3	0.11985	11.51	11.56	13.10
72	2.5	0.12198	13.49	13.55	15.11
90	2	0.12540	16.67	16.73	18.34

critical thickness. Thus, simulations have been finally produced for reasonable physical values of material parameters for masonry but such values should not have affected the obtained results. Failure of the arch shall be basically ruled by equilibrium and, in Heyman's sense, when the arch does not have enough thickness to withstand its self-weight, it fails, despite its stiffness/compliance properties. However, it is true that the present are real numerical simulations and that different simulation parameters may play a role (for example in the slight shift of critical thickness estimation) but it is hard to decipher which specific parameters may be, of the ones that could not be controlled by the user in the adopted computational tool.

In the present numerical simulations two main parameters at the user's disposal intervene in controlling the time stepping procedure: the "*Number of Timesteps*" and the "*Max Displacement per Timestep Ratio*". The first sets the duration of the simulation and, in the present analysis, it may be changed in view of reaching collapse at variable geometrical characteristics and number of blocks of the arch (see Section 3.2). The second plays a role in the algorithm that automatically fixes the current timestep and in that which detects the contact among adjacent blocks. In the final simulations that are reported in this work, this parameter has been fixed to 0.001, i.e. in the range of values suggested in the documentation manual. Further details on contact handling

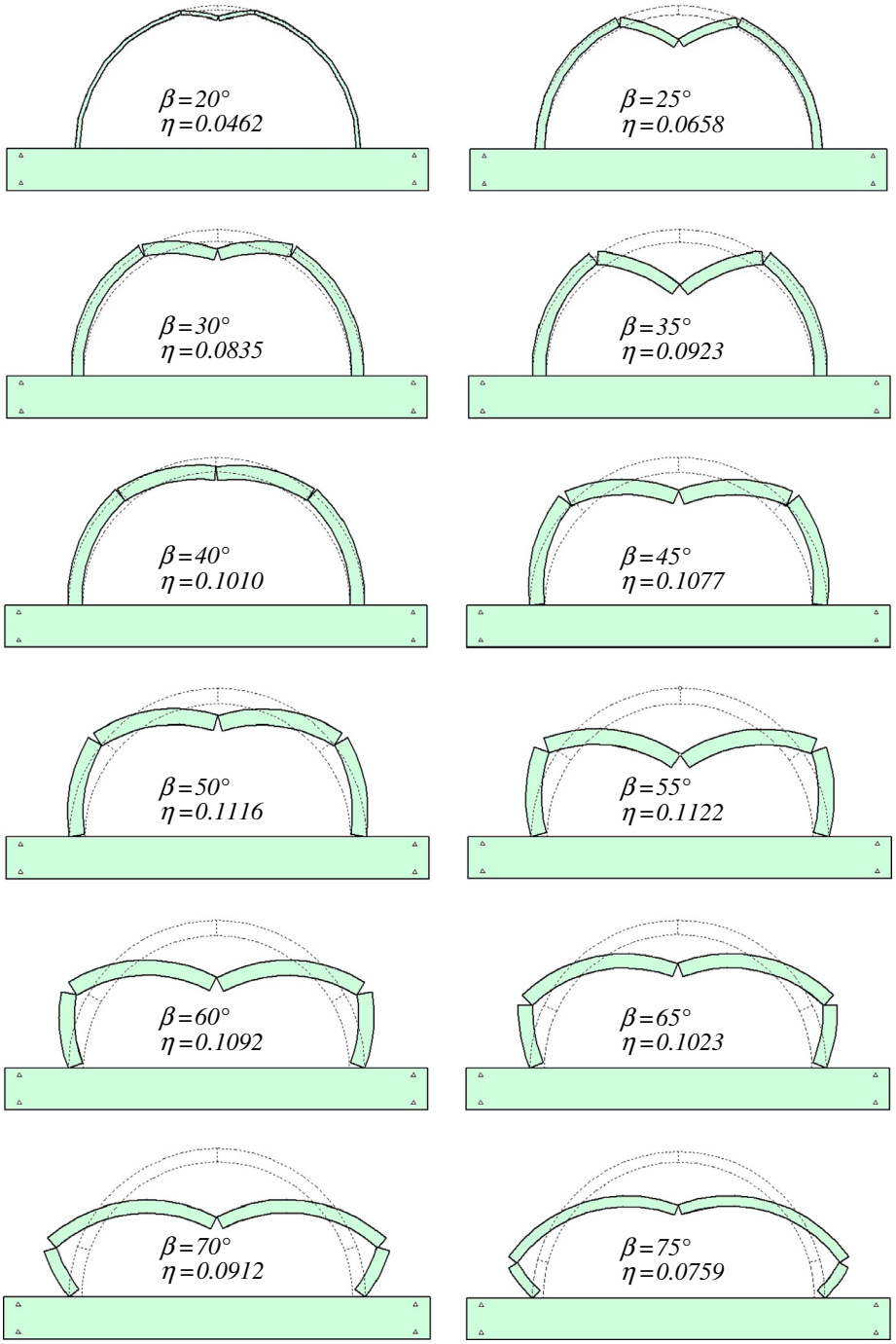

Fig. 12. DDA collapse modes of a complete semi-circular arch ($\alpha = 90°$) made with 4 blocks; so-imposed joint position β and resulting critical η.

algorithms and convergence criteria in the realm of DDA formulations may be found in Yeung et al. [63,64], Jiang and Yeung [35], and Jiang et al. [36].

3.1. Influence of the friction coefficient at the joints

A first investigation has concerned the role of the friction coefficient $\mu = \tan\varphi$ at the joints of the arch's voussoirs, especially towards the resulting manifestation of the collapse mode. Indeed, the earlier-adopted Heyman hypothesis-1 ruling-out sliding failure (thus necessarily leading to a purely-rotational collapse mode) looks fairly reasonable for masonry structures, at least in ideal conditions, but might fade-down at decreasing friction.

In this respect, Gilbert et al. [26] obtain, through a numerical approach, a purely-rotational collapse mode for friction coefficients μ larger than 0.396 (friction angle φ greater than $\varphi = 21.60°$), which should mark the transition between purely-rotational and sliding/rotational modes. The transition between sliding/rotational and purely-sliding mechanisms is instead signalled at $\mu = 0.31$ ($\varphi = 17.22°$). These results appear quite in agreement with those provided earlier by Sinopoli et al. [52], which provide for the above-mentioned bounds the values of $\mu = 0.395$ ($\varphi = 21.55°$) and $\mu = 0.309$ ($\varphi = 17.17°$).

In view of enquiring numerically the role of friction at the joints, mainly for finding the threshold value of friction coefficient from which only purely-rotational collapse modes appear, a few analyses have been run with different friction coefficients at the joints of a complete semi-circular arch ($\alpha = 90°$), with implemented slightly-sub-critical thickness coming from the theoretical analysis on purely-rotational collapse modes according to classical Heyman's solution, $\eta_H = 0.105965$ (thus truly sub-critical, since $\eta_{CCR} = 0.107426$ and $\eta_M = 0.107478$), discretised with 36 blocks (arch voussoirs of 5° opening).

Specifically, main results have been condensed in Fig. 8, where four characteristic values of friction angle φ have been considered: $\varphi = 0°, 10°, 20°, 30°$ ($\mu = 0, 0.176, 0.364, 0.577$). In good agreement with what reported in the literature above (and in the recent analysis in Frigerio [24], Colasante [15], Rizzi et al. [49] the recorded collapse modes turn-out as follows: purely-sliding collapse for $\varphi = 0°$ (no friction); mainly-sliding collapse for $\varphi = 10°$; mixed sliding-rotational collapse for $\varphi = 20°$ (value that should lie indeed within the range of mixed modes); purely-rotational mechanism for $\varphi = 30°$ (value that should be already high enough to prevent sliding). Thus, in view of reproducing just purely-rotational modes, all subsequent analyses have been run with a high value of friction angle, $\varphi = 50°$ ($\mu = 1.192$), that appears apt to comply numerically with Heyman's hypothesis-1. The so-obtained purely-rotational collapse modes agree quite well qualitatively with what predicted by theory, displaying extrados hinges at the crown and at the shoulders and intrados hinges at the haunches.

3.2. Evaluation of inner hinge location

In a second series of numerical tests, again complete semi-circular arches ($\alpha = 90°$) with implemented critical thicknesses from both Heyman's ($\eta_H = 0.105965$) and CCR ($\eta_{CCR} = 0.107426$) solutions, made with variable number of blocks (24, 30, 36, 60, 72, 90, 108, 144, 180), i.e. with (7.5°, 6°, 5°, 3°, 2.5°, 2°, 5/3° = 1.67°, 1.25°, 1°) voussoir openings, have been analysed. The purpose of the analyses was specifically that of investigating the angular position β of the resulting inner hinge at the haunches, as compared to the values coming from the three analytical solutions (though expected to be quite near to each other).

Results in terms of β turned-out to be independent of either choice of $\eta = \eta_H$ or $\eta = \eta_{CCR}$, which appears consistent with the theoretical treatment, since both values of η appear sub-critical with

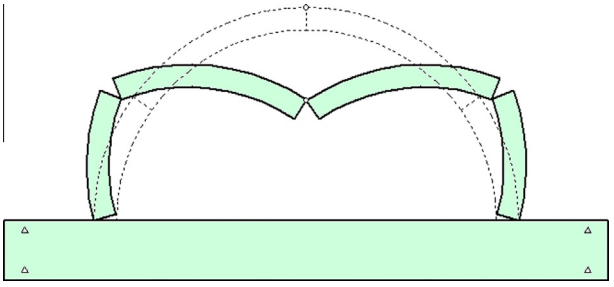

Fig. 13. DDA collapse mode of a complete semi-circular arch ($\alpha = 90°$) made with 4 blocks; sample with so-imposed joint at $\beta = 54.5°$, resulting critical $\eta = 0.1123$.

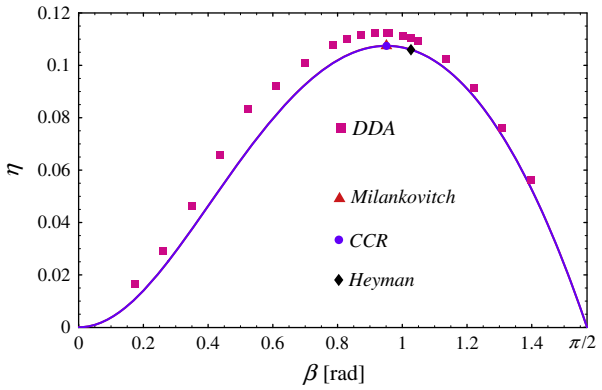

Fig. 14. Numerical DDA (4 blocks) vs. analytical results of $\eta(\beta)$ necessary for equilibrium at given intrados hinge β ($\alpha = 90°$). Results also in Table 2.

Table 3
DDA vs. analytical solutions for an over-complete circular arch ($\alpha = 140°$) made with 4 blocks (see samples in Figs. 15 and 16). Critical thickness to radius ratio η at first collapse instance at so-imposed β joint; results also plotted in Fig. 17.

Hinge position		DDA	Milankovitch		CCR/Heyman	
β		η	$\eta(\beta)$	Δ	$\eta(\beta)$	Δ
(deg)	(rad)	(1)	(1)	(%)	(1)	(%)
10	0.174533	0.35025	0.343226	2.05	0.327072	7.09
20	0.349066	0.46124	0.456790	0.97	0.436138	5.76
30	0.523599	0.54531	0.542821	0.46	0.521221	4.62
40	0.698132	0.60005	0.598098	0.33	0.579065	3.62
50	0.872665	0.62912	0.627155	0.31	0.612580	2.70
59.0	1.02974	0.63585	0.634867	0.15	0.624665	1.79
60	1.04720	0.63575	0.634772	0.15	0.625041	1.71
61.5	1.07338	0.63572	0.634293	0.22	0.625256	1.67
70	1.22173	0.62555	0.624268	0.21	0.618830	1.09
80	1.39626	0.59780	0.597296	0.08	0.595150	0.45
85.7	1.49575	0.57547	0.574663	0.14	0.573882	0.28
90	1.57080	0.55515	0.553992	0.21	0.553992	0.21
100	1.74533	0.49353	0.493089	0.09	0.494128	−0.12
110	1.91986	0.41241	0.411915	0.12	0.413070	−0.16
120	2.09440	0.30848	0.306330	0.70	0.307020	0.48

respect to Milankovitch solution ($\eta_M = 0.107478$), which should be the nearest to reality. Furthermore, as expected, the numerical outcomes have also displayed overall a hinge position β that is definitely more on the side of Milankovitch ($\beta_M = 54.4840°$) and CCR ($\beta_{CCR} = 54.4963°$) solutions, rather than on Heyman's solution ($\beta_H = 58.8293°$).

Indeed, salient results have been resumed in Figs. 9 and 10, where, respectively, the various obtained rotational collapse

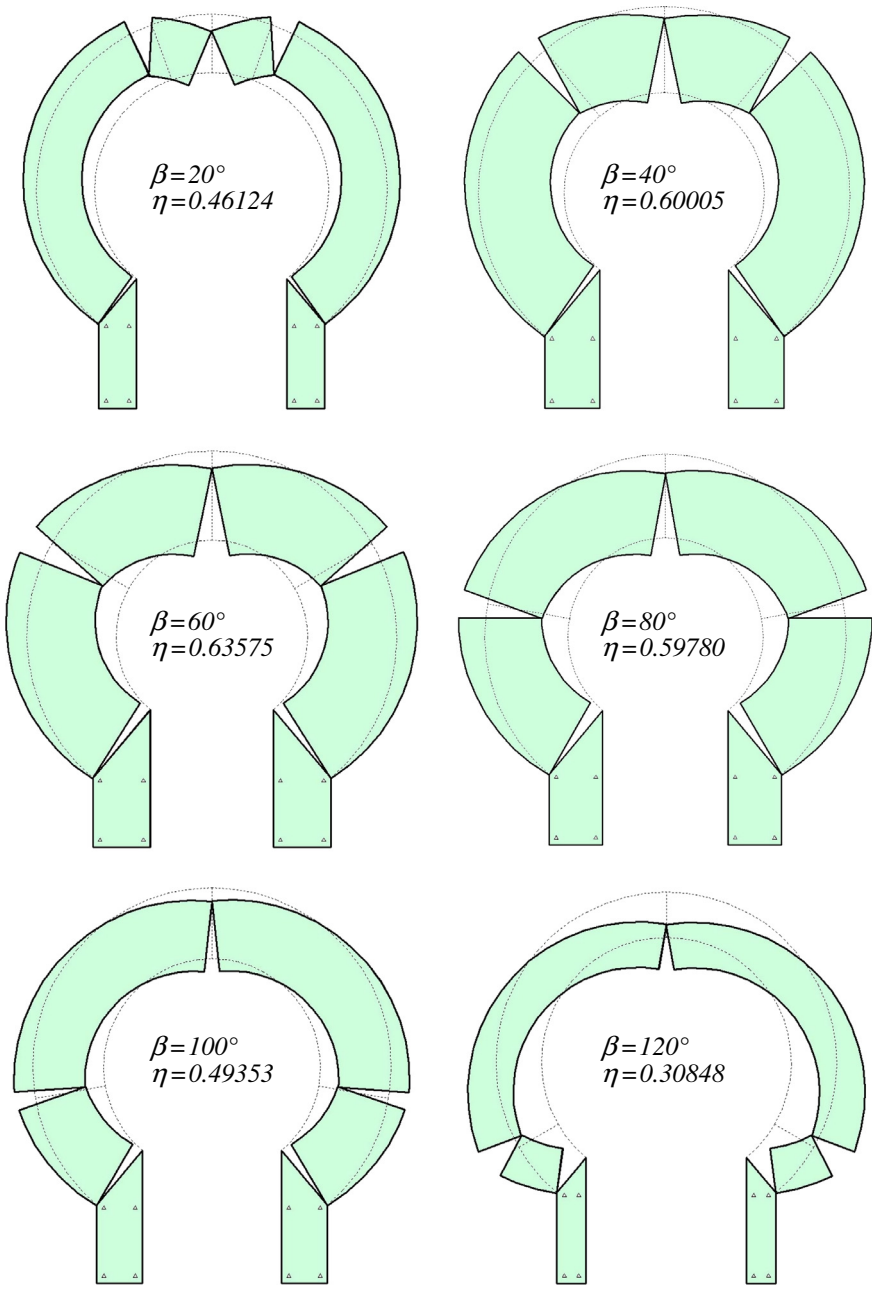

Fig. 15. DDA collapse modes of an over-complete circular arch ($\alpha = 140°$) made with 4 blocks; so-imposed joint position β and resulting critical η.

modes are reported, with relevant estimation of the angular inner hinge position, and the resulting plot of angular position β as a function of number of blocks is displayed. The latter shows rather an agglomeration of points scored by the DDA numerical solution that are located around the theoretical values predicted by Milankovitch and CCR solutions. The cases with least and largest number of blocks appear to detach a bit from the theoretical predictions, the first being expected since the theoretical locations of the joints are restricted to occur only each 7.5°, the second probably because the behaviour of the discrete system at increasing number of blocks is representing (contrary to what is customary in mesh refinement in FEM analyses) more and more that of a discontinuous structural medium rather than of a continuum, as it has been conceived in the theoretical analysis. Further comments on this aspect are also outlined in the following section. The numerical analyses require an increasing number of time steps at increasing number of blocks, ranging from 1000 for the arch with 24 blocks to 4000 for the arch with 180 blocks.

3.3. Evaluation of critical thickness

A third campaign of analyses has been attempted to determine the critical value of thickness to radius ratio η leading to the first instance of collapse, still for full semi-circular arches ($\alpha = 90°$), made again with variable number of blocks, namely (12, 18, 24, 30, 36, 60, 72, 90), i.e. with (15°, 10°, 7.5°, 6°, 5°, 3°, 2.5°, 2°) voussoir openings. In each instance, the thickness has been decreased gradually, until collapse has arisen for the first time at reducing thickness. In getting the fork of values around the critical condition, the value of η corresponding to the first collapse occurrence has been annotated.

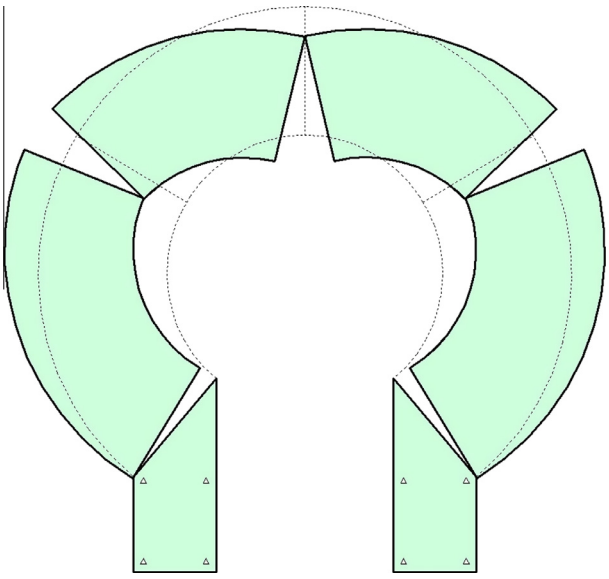

Fig. 16. DDA collapse mode of an over-complete circular arch ($\alpha = 140°$) made with 4 blocks; sample with so-imposed joint at $\beta = 59°$, resulting critical $\eta = 0.63585$.

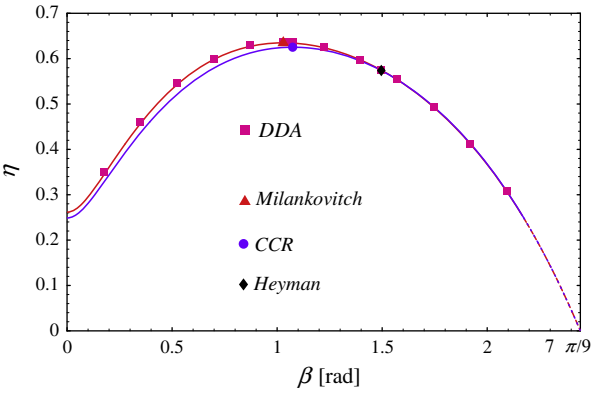

Fig. 17. Numerical DDA (4 blocks) vs. analytical results of $\eta(\beta)$ necessary for equilibrium at given intrados hinge β ($\alpha = 140°$). Results also in Table 3.

The obtained numerical results are shown in Table 1 and depicted in Fig. 11, with comparison to the three analytical solutions. Notice that the DDA scores are always above the theoretical predictions and tend to diverge from them, almost linearly, at increasing number of blocks. This might be explained in terms of a response of a continuum that is turning more and more into a discontinuum, whereby the DDA simulation represents the response of a true discrete system of blocks. Actually, this discrepancy is quite emphasised in the tight zoom window of η values in the range around the expected theoretical values, as represented in Fig. 11; less difference would be appreciated visually in larger η windows from 0 to the experienced larger value at around 0.125, or even more in η windows from 0 to 1. Table 1 indeed shows that the highest difference, to Milankovitch solution, displays a value of about 17% for the case of 90 blocks (with 2° opening), while more confined differences below 7% are recorded for more realistic chunks with openings that are larger than 5°.

In any case, the relative distance between DDA and Milankovitch/CCR solutions appears to be always less than the distance between DDA and Heyman's solution (i.e. Milankovitch/CCR predictions are always between Heyman's estimate and DDA numerical evaluations). This agreement further validates in academic terms Milankovitch/CCR solutions vs. Heyman's solution, Milankovitch being the nearest to DDA results.

Table 4
DDA vs. analytical solutions at variable half-angle of embrace of the arch (voussoirs with 5° opening); results also plotted in Figs. 19 and 20.

Arch opening		Numerical vs. analytical solutions				
α		$\beta_{DDA/M/CCR/H}$			$\eta_{DDA/M/CCR/H}$	
(deg)	(rad)	(deg)	(rad)	Δ (%)	(1)	Δ (%)
45	0.785398	30	0.523599	–	0.01680	–
		30.5146	0.532580	−1.69	0.00749612	+124.12
		30.5146	0.532581	−1.69	0.00749609	+124.12
		31.0935	0.542684	−3.52	0.00748686	+124.39
60	1.04720	40	0.698132	–	0.03077	–
		39.4606	0.688718	+1.37	0.0228489	+34.67
		39.4608	0.688721	+1.37	0.0228482	+34.67
		40.7902	0.711924	−1.94	0.0227694	+35.14
75	1.30900	45	0.785398	–	0.06030	–
		47.5008	0.829045	−5.26	0.0536896	+12.31
		47.5027	0.829079	−5.27	0.0536818	+12.33
		50.0339	0.873256	−10.06	0.0532849	+13.17
90	1.57080	55	0.959931	–	0.11303	–
		54.4840	0.950925	+0.95	0.107478	+5.17
		54.4963	0.951141	+0.92	0.107426	+5.22
		58.8293	1.02677	−6.51	0.105965	+6.67
100	1.74533	60	1.04720	–	0.16559	–
		58.4309	1.01981	+2.69	0.160736	+3.02
		58.4674	1.02045	+2.62	0.160584	+3.12
		64.4657	1.12514	−6.93	0.157463	+5.16
110	1.91986	60	1.04720	–	0.23714	–
		61.6327	1.07569	−2.65	0.232295	+2.09
		61.7328	1.07744	−2.81	0.231885	+2.27
		69.9447	1.22077	−14.22	0.225573	+5.13
120	2.09440	65	1.13446	–	0.33290	–
		63.7402	1.11248	+1.98	0.327607	+1.62
		64.0072	1.11714	+1.55	0.326547	+1.95
		75.2920	1.31409	−13.67	0.314124	+5.98
130	2.26893	65	1.13446	–	0.46174	–
		63.8795	1.11491	+1.75	0.455450	+1.38
		64.6207	1.12784	+0.59	0.452593	+2.02
		80.5361	1.40562	−19.29	0.428043	+7.87
140	2.44346	60	1.04720	–	0.64303	–
		58.9760	1.02933	+1.74	0.634867	+1.29
		61.5313	1.07392	−2.49	0.625256	+2.84
		85.7066	1.49586	−29.99	0.573854	+12.05
145	2.53073	50	0.872665	–	0.77467	–
		49.6698	0.866901	+0.66	0.763995	+1.40
		56.2271	0.981348	−11.07	0.740638	+4.60
		88.2735	1.54066	−43.36	0.661358	+17.13

3.4. Analyses at pre-imposed inner hinge location

Furthermore, circular arches with only four blocks have been considered, with joints at the crown and at the shoulders and with an inner joint at given variable angular position β. Equilibrium states have been investigated with a so-imposed β joint at decreasing thickness of the arch, until collapse has arisen for the first time for a recorded critical value of η, in view of determining the critical value of η at a given potential position of the inner hinge at the haunches.

Full semi-circular arches have been considered first ($\alpha = 90°$), which should lead to trends of the equilibrium curve $\eta(\beta)$ similar to those already displayed in Fig. 6; then, over-complete arches with $\alpha = 140°$ have been modelled, with expected trends of $\eta(\beta)$ as those previously represented in Fig. 7.

These analyses also showed quite good agreement with the analytical treatment. Results for $\alpha = 90°$ are first gathered in Table 2

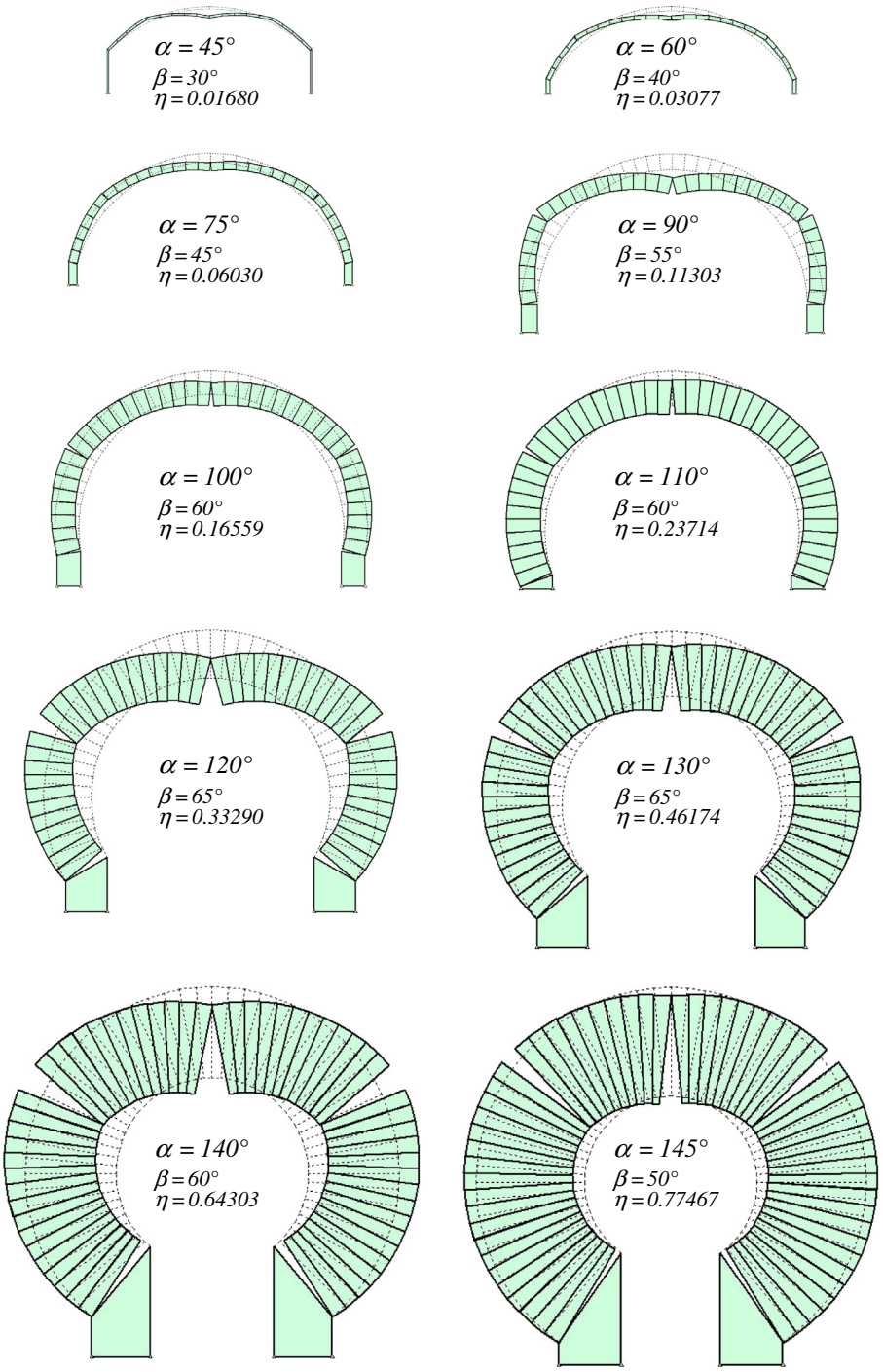

Fig. 18. DDA collapse modes of circular masonry arches with variable half-angle of embrace α, made with blocks with 5° opening; recorded angular position β of the inner intrados hinge at the haunches and critical thickness to radius ratio η.

and depicted in Figs. 12–14. The bell-shaped trend of the curve $\eta(\beta)$ is reproduced quite well. A little over-shooting in terms of critical η is again displayed by the points scored by the DDA solution (quite visible in a tight η window between 0 and 0.12), more for low and pre-peak values of β, less for post-peak values (see also Table 2, where the percentage variation in thickness estimate may become higher than 10% just for β less than about 40°). As seen in the previous subsection, the numerical DDA solution of a discontinuous system of discrete blocks appears a little bit more unstable than the theoretical solution corresponding to an ideal continuous arch. However, the maximum of the curve $\eta(\beta)$ is estimated quite reasonably, with a deviation from Milankovitch/CCR solutions that is only about 4.5% (see details in Table 2). Also, the angular location β of the numerical peak is again very near to the prediction from Milankovitch/CCR solutions and displaced from the estimate from Heyman's solution.

Similar results are obtained as well for the reference over-complete case of $\alpha = 140°$, as gathered in Table 3 and represented in Figs. 15–17. Notice the very good agreement with the theoretical predictions of the equilibrium curve $\eta(\beta)$ (now in a wider η window between 0 and 0.7), especially for Milankovitch prediction, including with the various discussed features attached to the limit value η_0 that $\eta \geqslant \eta_0$ may take for admissible equilibrium states of the arch, as it has been analysed in details in Section 2.1.

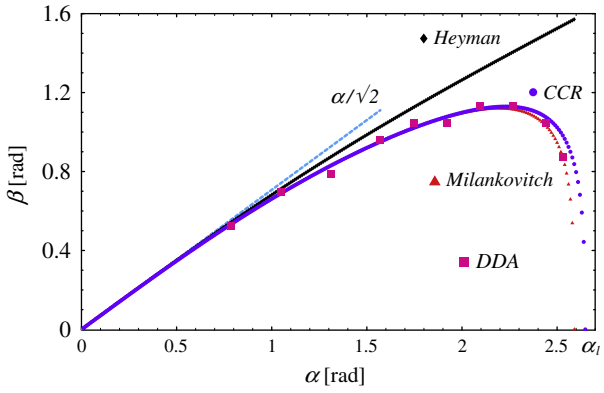

Fig. 19. Numerical DDA (blocks of 5° opening) vs. analytical solutions at variable half-angle of embrace α: angular position β of the inner hinge. Results also in Table 4.

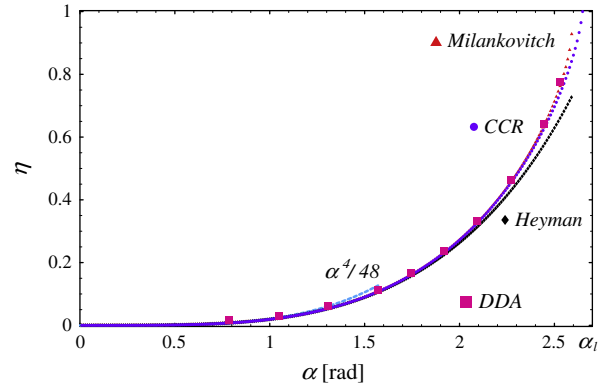

Fig. 20. Numerical DDA (blocks of 5° opening) vs. analytical solutions at variable half-angle of embrace α: thickness to radius ratio η. Results also in Table 4.

3.5. Simulations with different opening angles

Finally, discretised arches with different cut-off angles α have been considered, including cases of under-complete and over-complete arches, namely $\alpha = 45°$, 60°, 75°, 90°, 100°, 110°, 120°, 130°, 140°, 145°, made with discrete voussoirs with fixed 5° opening, to determine both critical β and η at the first collapse instance appearing at decreasing η.

The obtained DDA results are reported in Table 4, with collapse modes illustrated in Fig. 18 and relevant DDA critical values scored in the plots depicted in Figs. 19 and 20, with comparison to results from the three analytical solutions (and relevant trends for α small). These outcomes actually represent, characterise and summarise the main results of the present work. Indeed, the achieved data show a very good agreement between numerical DDA simulations and analytical solutions, especially, as expected, with respect to Milankovitch and CCR solutions stating the correct tangency condition on the true line of thrust.

Specifically, the true, newly-derived trends of $\beta(\alpha)$ in Milankovitch and CCR solutions, through a stationary point $\beta_{s\beta}(\alpha_{s\beta})$, are confirmed, as opposed to the monotonic increasing trend predicted by Heyman's solution in terms of β. The monotonic increasing trend of $\eta(\alpha)$ is also very well recovered by the DDA simulations, which, once more, always slightly over-predict the critical values of η, being nearer in any case to the outcomes of Milankovitch solution. Notice that, in the represented window of η between 0 and 1, the discrepancies between DDA and theoretical solutions are less visible, with respect to those that have been represented earlier in Figs. 11, 14 and 17 (see comments already drawn in Section 3.3).

As a general comment, the results depicted in Figs. 14 and 17 represent higher discrepancy to the analytical trends for lower values of β. This may be expected, since the block near the crown gets smaller and much wedge shaped. However, results shall be considered as quite satisfactory and representative in the present aim of validating the theoretical analysis. The purpose of this specific analysis is that of enquiring the critical value of thickness at imposed inner hinge location for a theoretical continuous arch. For this reason the arch has been divided just into four blocks, so as to pre-impose the position of the rupture joints and the analysis adheres to the analytical derivation developed in the paper. It is the opinion of the Authors that, by basically taking the DDA formulation as is and without specific tools to improve numerical performance, the match between numerical results and analytical outcomes is quite astonishing in Figs. 14 and 17 and in Figs. 19 and 20. Indeed, these condense and represent the core results of the present work.

Also, for the two benchmark cases extensively analysed in the paper for half opening angles $\alpha = 90°$ and $\alpha = 140°$, Figs. 13 and 16 represent the recorded numerical collapse mode of the arch, as detected by the present numerical DDA analysis. Indeed, in these cases the inner hinge leads to the maximum value of least thickness, as depicted in Figs. 14 and 17 and also represent very good matching with the theoretical results.

4. Closing remarks

This paper has presented an analytical and numerical analysis of the classical Couplet–Heyman problem in the statics of circular masonry arches. In the spirit of Heyman's studies and based on his classical behavioural hypotheses (leading to purely-rotational collapse modes), new analytical solutions have been reported, which correctly re-state the tangency condition at the haunches' intrados in terms of the true line of thrust (locus of pressure points). This leads to a variation of the inner hinge position, which can be much and much appreciated at increasing opening angle of the arch, especially for rather unusual over-complete arches. At the same time, the correct estimate of critical thickness shows, in academic terms, that Heyman's solution turns-out sub-critical, in the sense that it predicts a thickness to radius ratio that is smaller than that which should be truly required for equilibrium under self-weight.

Such analytical solutions have been assessed and confirmed by the parallel numerical DDA computations that have been reported here. These numerical simulations have produced results that, specifically for the true location of the inner hinge position at the haunches in the critical condition, and also for the evaluation of the minimum thickness to radius ratio, are overall in great agreement with the new outcomes of both Milankovitch and CCR solutions, rather than with classical results provided by Heyman's solution. This further supports the validity of these newly-derived analytical trends. Such analytical solutions have been re-derived independently in the paper, by emphasising explicitly the role of least thickness as the stationary condition leading to the maximum point of the equilibrium curve $\eta(\beta)$ that represents the limit of equilibrium states of the arch at decreasing thickness ratio η, at a given angular inner hinge position β.

Acknowledgements

This work has been carried-out at the University of Bergamo, Department of Engineering (Dalmine). The financial support by "*Fondi di Ricerca d'Ateneo ex 60%*" at the University of Bergamo is gratefully acknowledged. The work of people that have developed

and made available in internet for free the DDA program employed here is also very much acknowledged.

References

[1] Albuerne A, Williams M, Lawson V. Prediction of failure mechanism of arches and barrel vaults under base motion using the NSCD method. In: Jasieńko J, editor. Proc of 8th int conference on structural analysis of historical constructions, SAHC 2012. Wroclaw, Poland: DWE; October 15–17, 2012. p. 397–406.

[2] Audenaert A, Fanning P, Sobczak L, Peremans H. 2-D analysis of arch bridges using an elasto-plastic material model. Eng Struct 2008;30(3):845–55.

[3] Armesto J, Roca-Pardiñas J, Lorenzo H, Arias P. Modelling masonry arches shape using terrestrial laser scanning data and nonparametric methods. Eng Struct 2010;32(2):607–15.

[4] Bičanič N, Stirling C, Pearce CJ. Discontinuous modelling of masonry bridges. Comput Mech 2003;31(1–2):60–8.

[5] Blasi C, Foraboschi P. Analytical approach to collapse mechanisms of circular masonry arch. J Struct Eng ASCE 1994;120(8):2288–309.

[6] Block P, Ciblac T, Ochsendorf J. Real-time limit analysis of vaulted masonry buildings. Comput Struct 2006;84(29–30):1841–52.

[7] Boothby TE. Analytical approach to collapse mechanisms of circular masonry arch. Discussion on the paper by Blasi and Foraboschi (1994), with Closure by P. Foraboschi and C. Blasi. J Struct Eng ASCE 1996;122(8):978–80.

[8] Burman BC. A numerical approach to the mechanics of discontinua. Ph.D. thesis. Townsville, Australia: James Cook University of North Queensland; 1971.

[9] Cavicchi A, Gambarotta L. Lower bound limit analysis of masonry bridges including arch–fill interaction. Eng Struct 2007;29(11):3002–14.

[10] Cecchi A. The "Arch of equilibration" of Charles Hutton (1772). Meccanica 2010;45(6):829–33.

[11] Cecchi A. The curve of pressure in vertically loaded arches. In: Jasieńko J, editor. Proc of 8th int conference on structural analysis of historical constructions, SAHC 2012. Wroclaw, Poland: DWE; October 15–17, 2012. p. 457–64.

[12] Chen Y, Ashour AF, Garrity SW. Modified four-hinge mechanism analysis for masonry arches strengthened with near-surface reinforcement. Eng Struct 2007;29(8):1864–71.

[13] Cocchetti G, Colasante G, Rizzi E. On the analysis of minimum thickness in circular masonry arches. Part I: state of the art and Heyman's solution. Part II: present CCR solution. Part III: Milankovitch-type solution. Appl Mech Rev ASME 2011; 64(5): 051002, 27 pages. doi:http://dx.doi.org/10.1115/1.4007417 [ASME, New York, USA, 2012].

[14] Colasante G. Sui meccanismi di collasso degli archi in muratura secondo l'analisi limite. Laurea Thesis in Building Engineering, Advisor E. Rizzi, Co-Advisor G. Cocchetti, Università di Bergamo, Facoltà di Ingegneria, I-24044 Dalmine (BG), Italy; December 2007. 175 pages.

[15] Colasante G. Sul ruolo dell'attrito nei meccanismi di collasso degli archi circolari in muratura. Laurea (Master) Thesis, Advisor E. Rizzi, Co-Advisor G. Cocchetti, Università di Bergamo, Facoltà di Ingegneria, Italy; September 2010. 213 pages.

[16] Cundall PA. A computer model for simulating progressive, large scale movements in blocky rock systems. In: Proc of the symposium of the international society for rock mechanics, vol. 1, Nancy, France; 1971. Paper no. II-8.

[17] Cundall PA, Strack ODL. A discrete numerical model for granular assemblies. Géotechinque 1979;29(1):47–65.

[18] Cundall PA, Hart RD. Numerical modelling of discontinua. Eng Comput 1992;9(2):101–13.

[19] Doolin M, Sitar N. Displacement accuracy of discontinuous deformation analysis method applied to sliding block. J Eng Mech ASCE 2002;128(11):1158–68.

[20] Doolin M, Sitar N. Time integration in discontinuous deformation analysis. J Eng Mech ASCE 2004;130(3):249–58.

[21] Drosopoulos GA, Stavroulakis GE, Massalas CV. Limit analysis of a single span masonry bridge with unilateral frictional contact interfaces. Eng Struct 2006;28(13):1864–73.

[22] Foce F. On the safety of the masonry arch. Different formulations from the history of structural mechanics. In: Huerta S, editor. Essays in the history of the theory of structures. Madrid: Instituto Juan de Herrera; 2005. p. 117–42.

[23] Foce F. Milankovitch's Theorie der Druckkurven: Good mechanics for masonry architecture. Nexus Netw J 2007;9(2):185–210.

[24] Frigerio A. Sul meccanismo di collasso misto negli archi semicircolari in muratura. Laurea Thesis in Building Engineering, Advisor E. Rizzi, Co-Advisor G. Colasante, Università di Bergamo, Facoltà di Ingegneria, Italy; March 2010. 130 pages.

[25] Gago AS, Alfaiate J, Lamas A. The effect of the infill in arched structures: analytical and numerical modelling. Eng Struct 2011;33(5):1450–8.

[26] Gilbert M, Casapulla C, Ahmed HM. Limit analysis of masonry block structures with non-associative frictional joints using linear programming. Comput Struct 2006;84(13–14):873–87.

[27] Giordano A, Mele E, De Luca A. Modelling of historical masonry structures: comparison of different approaches through a case study. Eng Struct 2002;24(8):1057–69.

[28] Gubana A, Di Gianantonio I. Triumphal arch collapse mechanisms. In: Jasieńko J, editor. Proc of 8th int conference on structural analysis of historical constructions, SAHC 2012. Wroclaw, Poland: DWE; October 15–17, 2012. p. 253–61.

[29] Hahn JK. Realistic animation of rigid bodies. Comput Graph (Proc SIGGRAPH 1988) 1988;22(4):299–308.

[30] Heyman J. The safety of masonry arches. Int J Mech Sci 1969;11(4):363–85.

[31] Heyman J. Equilibrium of shell structures. Oxford: Oxford University Press; 1977.

[32] Heyman J. The masonry arch. Chichester: Ellis Horwood Ltd.; 1982.

[33] Heyman J. La coupe des pierres. In: Proceedings of the third international congress on construction history, vol. 2. Cottbus, Germany: Brandenburg University of Technology; 20–24 May 2009. p. 807–12.

[34] Holzer SM. Numerical arch and vault analysis. In: Jasieńko J, editor. Proc of 8th int conference on structural analysis of historical constructions, SAHC 2012. Wroclaw, Poland: DWE; October 15–17, 2012. p. 77–93.

[35] Jiang QH, Yeung MR. A model of point-to-face contact for three-dimensional discontinuous deformation analysis. Rock Mech Rock Eng 2004;37(2):95–116.

[36] Jiang QH, Chen YF, Zhou CB, Yeung MR. Kinetic energy dissipation and convergence criterion of discontinuous deformations analysis (DDA) for geotechnical engineering. Rock Mech Rock Eng 2013;46(6):1443–60.

[37] Kooharian A. Limit analysis of voussoir (segmental) and concrete arches. J Am Concr Inst 1952; 24(4), Proc 49(12): 317–328. Title no. 49-24.

[38] Lemos JV, Hart RD, Cundall PA. A generalized distinct element program for modelling jointed rock mass. In: Proc of int symposium on fundamentals of rock joints, Björkliden, Luleå, Sweden, Centek; 1985. p. 335–43.

[39] Lemos JV. Discrete element modeling of masonry structures. Int J Architect Heritage 2007;1(2):190–213.

[40] Lin CT, Amadei B, Jung J, Dwyer J. Extensions of discontinuous deformation analysis for jointed rock masses. Int J Rock Mech Min Sci Geomech Abstracts 1996;33(7):671–94.

[41] Ma MY, Pan AD, Luan M, Gebara JM. Stone arch bridge analysis by the DDA method. In: Melbourne C, editor. Proc of 1st int conf on arch bridges. Bolton, UK: Thomas Telford Ltd.; 3–6 September 1995. p. 247–56.

[42] MacLaughlin MM, Doolin DM. Review of validation of the discontinuous deformation analysis (DDA) method. Int J Numer Anal Methods Geomech 2006;30(4):271–305.

[43] Maini T, Cundall PA, Marti J, Beresford NL, Asgian M. Computer modeling of jointed rock masses. Technical report N-78-8. U.S. Army Waterways Experiment Station, Vicksburg, MS; August 1978.

[44] Milankovitch M. Theorie der Druckkurven. Z Math Phys 1907;55:1–27.

[45] Ochsendorf J. Collapse of masonry structures. Doctoral dissertation. UK: University of Cambridge, King's College; 2002.

[46] Ochsendorf J. The masonry arch on spreading supports. Struct Eng 2006;84(2):29–36.

[47] Oliveira DV, Lourenço PB, Lemos C. Geometric issues and ultimate load capacity of masonry arch bridges from the northwest Iberian Peninsula. Eng Struct 2010;32(12):3955–65.

[48] Rizzi E, Cocchetti G, Colasante G, Rusconi F. Analytical and numerical analysis on the collapse mode of circular masonry arches. In: Proc of 7th int conference SAHC 2010, vols. 133–134. Shanghai, China: Advanced Materials Research, Trans Tech Publications; October 6–8, 2010. p. 467–72.

[49] Rizzi E, Colasante G, Frigerio A, Cocchetti G. On the mixed collapse mechanism of semi-circular masonry arches. In: Jasieńko J, editor. Proc of 8th int conference on structural analysis of historical constructions, SAHC 2012. Wroclaw, Poland: DWE; October 15–17, 2012. p. 541–9.

[50] Rusconi F. Analisi numerica per elementi discreti dei meccanismi di collasso degli archi in muratura. Laurea Thesis in Building Engineering, Advisor E. Rizzi, Università di Bergamo, Facoltà di Ingegneria, I-24044 Dalmine (BG), Italy; February 2008; 126 pages.

[51] Sacco E. Stress approaches for the analysis of masonry arches. In: Jasieńko J, editor. Proc of 8th int conference on structural analysis of historical constructions, SAHC 2012. Wroclaw, Poland: DWE; October 15–17, 2012. p. 550–8.

[52] Sinopoli A, Corradi M, Foce F. Modern formulation for preelastic theories on masonry arches. J Eng Mech ASCE 1997;123(3):204–13.

[53] Shi G-H, Goodman RE. Discontinuous deformation analysis. In: Proc of 25th U.S. symposium on rock mechanics, SME/AIME, Evanston, IL, USA; 1984. p. 269–77.

[54] Shi G-H, Goodman RE. Two dimensional discontinuous deformation analysis. Int J Numer Anal Methods Geomech 1985;9(6):541–56.

[55] Shi G-H. Discontinuous deformation analysis – a new numerical model for the statics and dynamics of block systems. Ph.D. thesis. Berkeley: University of California; 1988.

[56] Shi G-H. Block system modeling by discontinuous deformation analysis. Topics in engineering. Southampton, UK: Computational Mechanics Publications; 1993.

[57] Solla M, Caamaño JC, Riveiro B, Arias P. A novel methodology for the structural assessment of stone arches based on geometric data by integration of photogrammetry and ground-penetrating radar. Eng Struct 2012;35:296–306.

[58] Tóth AR, Orbán Z, Bagi K. Discrete element analysis of a stone masonry arch. Mech Res Commun 2009;36(4):469–80.

[59] Thavalingam A, Bičanič N, Robinson JI, Ponniah DA. Computational framework for discontinuous modelling of masonry arch bridges. Comput Struct 2001;79(19):1821–30.
[60] Wang CY, Chuang CC, Sheng J. Time integration theories for the DDA method with finite element meshes. In: Salami MR, Banks D, editors. Proc of 1st int forum on discontinuous deformation analysis and simulations of discontinuous media. Berkeley, CA TSI, Albuquerque; 1996. p. 263–87.
[61] Williams JR, Hocking G, Mustoe GGW. The theoretical basis of the discrete element method. In: NUMETA'85, numerical methods in engineering, theory and applications. Rotterdam: Balkema; 1985.
[62] Williams JR, Mustoe GGW. Modal methods for the analysis of discrete systems. Comput Geotech 1987;4(1):1–19.
[63] Yeung MR, Jiang QH, Sun N. Validation of block theory and three-dimensional discontinuous deformation analysis as wedge stability analysis methods. Int J Rock Mech Min Sci 2003;40(2):265–75.
[64] Yeung MR, Jiang QH, Sun N. A model of edge-to-edge contact for three-dimensional discontinuous deformation analysis. Comput Geotech 2007;34(3):175–86.